Accepted Manuscript

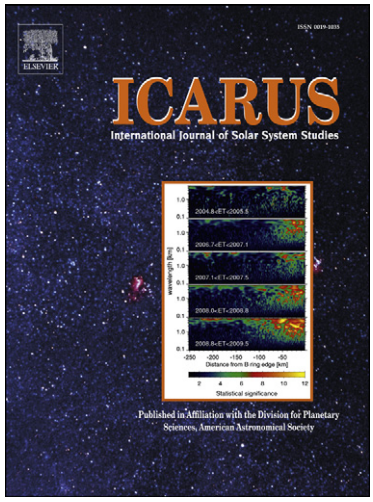

The origin and timing of fluvial activity at Eberswalde crater, Mars

N. Mangold, E.S. Kite, M.G. Kleinhans, H. Newsom, V. Ansan, E. Hauber, E. Kraal, C. Quantin, K. Tanaka

PII: S0019-1035(12)00208-4
DOI: http://dx.doi.org/10.1016/j.icarus.2012.05.026
Reference: YICAR 10233

To appear in: *Icarus*

Received Date: 19 September 2011
Revised Date: 2 May 2012
Accepted Date: 22 May 2012

Please cite this article as: Mangold, N., Kite, E.S., Kleinhans, M.G., Newsom, H., Ansan, V., Hauber, E., Kraal, E., Quantin, C., Tanaka, K., The origin and timing of fluvial activity at Eberswalde crater, Mars, *Icarus* (2012), doi: http://dx.doi.org/10.1016/j.icarus.2012.05.026

The origin and timing of fluvial activity at Eberswalde crater, Mars

N. Mangold (1), E.S. Kite (2), M. G. Kleinhans (3), H. Newsom (4), V. Ansan (1), E. Hauber (5), E. Kraal (6), C. Quantin (7), K. Tanaka (8).

(1) Laboratoire Planétologie et Géodynamique de Nantes, LPGN/CNRS, Université Nantes, 2, rue de la Houssinière, 44322 Nantes. nicolas.mangold@univ-nantes.fr

(2) Division of Geological and Planetary Science, Caltech MC 150-21, 1200 E. California Boulevard, Pasadena CA 91125, USA, ekite@caltech.edu

(3) Faculty of Geosciences, Universiteit Utrecht, PO Box 80115, 3508 TC Utrecht, The Netherlands, m.g.kleinhans@uu.nl

(4) Institute of Meteoritics and Dept. of Earth and Planetary Sciences, University of New Mexico, Albuquerque NM 87131, USA, newsom@unm.edu

(5) Institut für Planetenforschung / *Institute of Planetary Research* German Aerospace Center (DLR) Rutherfordstr. 2 12489 Berlin Germany, Ernst.Hauber@dlr.de

(6) Department of Physical Sciences, Kutztown University of Pennsylvania, USA, kraal@kutztown.edu

(7) Laboratoire Géologie de Lyon, La Doua, Université Claude Bernard Lyon, 69622, Villeurbanne, France, cathy.quantin-nataf@univ-lyon1.fr

(8) Astrogeology Science Center, U.S. Geological Survey, 2255 N. Gemini Dr. Flagstaff, AZ 86001, USA, ktanaka@usgs.gov

Highlights:

- Valleys feeding the Eberswalde fan crosscut Holden impact crater ejecta blanket.
- Holden crater formation likely postdates the Early Hesperian.
- Modeling shows Eberswalde fan can form at a geologically rapid rate.
- The role of Holden crater in Eberswalde fluvial activity is highlighted.

Abstract

The fan deposit in Eberswalde Crater has been interpreted as strong evidence for sustained liquid water on early Mars with a paleolake formed during the Noachian period (>3.7 Gy). This location became a key region for understanding the Mars paleo-environment. Eberswalde crater is located 50 km north of the rim of the 150 km diameter crater Holden. Stratigraphic relationships and chronology obtained using recent Mars Express High Resolution Stereo Camera and Mars Reconnaissance Orbiter Context Camera images show that Eberswalde fluvial activity crosscuts Holden ejecta and thus postdates Holden crater, whose formation age is estimated from crater counts as Late Hesperian (~3.5 Gy, depending on models). Fluvial modeling shows that short term activity (over several years to hundreds of years) involving dense flows (with sediment:water ratio between 0.01 and 0.3) may be as good an explanation of the fluvial landforms as dilute flow over longer durations. Modeling of the thermal effect of the Holden impact in the Eberswalde watershed is used to evaluate its potential role in aqueous activity. The relative timing of the Holden impact and Eberswalde's fan is a constraint for future studies about the origin of these landforms. Holden ejecta form a weak and porous substrate, which may be easy to erode by fluvial incision. In a cold climate scenario, impact heating could have produced runoff by melting snow or ground ice. Any attempt to model fluvial activity at Eberswalde should take into account that it may have formed as late as in the Late Hesperian, after the great majority of valley network formation and aqueous mineralization on Mars. This suggests that hypotheses for fan formation at Eberswalde by transient and/or localized processes (i.e. impact, volcanism, unusual orbital forcing) should be considered on a par with globally warmer climate.

1. Introduction

The discovery of a partially eroded fan deposit in Eberswalde Crater, north of the Holden crater has been interpreted as strong evidence for sustained liquid water on early Mars (Malin and Edgett, 2003). This fan is usually interpreted as a delta formed in a standing body of water (Malin and Edgett, 2003, Moore et al., 2003, Wood et al., 2006, Lewis and Aharonson, 2006, Pondrelli et al., 2008, Rice et al., 2011). Eberswalde crater is located 50 km north of the 150 km diameter crater Holden (Fig. 1). The latter shows various fluvial landforms too, including alluvial fans - as observed in many southern hemisphere large craters (Cabrol and Grin, 1999, Moore and Howard, 2005, Kraal et al., 2008a, Grant and Wilson, 2011) - and layered sediments that may correspond to a period of lacustrine deposition during the Noachian period (Grant et al., 2008). Both craters could thus represent a region in which early Mars fluvial and lacustrine activity is well-preserved. Locations on the floors of both craters were among the final four candidate locations for the Mars Science Laboratory landing site for this reason (Grant et al., 2010).

However, the processes and timescale for fluvial erosion and sedimentation at Eberswalde crater are actively debated. Alternatives to the delta theory include alluvial fan progradation onto a dry crater floor (Jerolmack et al., 2004), or emplacement as a dense viscous flow (Kraal and Postma, 2008). The time scales associated with these mechanisms range from a few years (Jerolmack et al., 2004) to >100,000 years (Bhattacharya et al., 2005). It remains unclear whether deposition of the fan occurred into standing water or not, and hydrologic modeling (Jerolmack et al., 2004) suggests deposition need not have persisted as long as originally inferred (e.g., Moore et al., 2003). Jerolmack et al. (2004)

proposed a link between the formation of Holden crater and the fluvio-lacustrine activity at Eberswalde, but no observations were ever made to link these processes together.

In the present study, we use new data from the High Resolution Stereo Camera (HRSC, Neukum et al., 2004) onboard Mars Express, and the Context Camera (CTX, Malin et al., 2007) and the High Resolution Imaging Science Experiment (HiRISE, Mc Ewen et al., 2007) onboard Mars Reconnaissance Orbiter, to:- (1) establish the relative stratigraphic relationships between Holden ejecta, Eberswalde fluvial landforms and other regional landforms; (2) constrain the absolute chronology of these processes using crater counts; (3) study the hydrology of the Eberswalde catchment using new HRSC Digital Elevation Models (DEMs) and analyze implications for the stratigraphy; (4) finally, discuss formation hypotheses (a globally warmer climate, or other processes) in light of the stratigraphic constraints. Our observations show that the valleys feeding Eberswalde's fan delta crosscut Holden ejecta, thus post-dating Holden crater formation, while Holden's age is estimated as being Hesperian on the basis of crater counts. Our results show that mapping and detection of ancient crater ejecta can be a powerful tool in identifying cross-cutting relationships between ancient fluvial landforms and determining their age.

2. Data and Methods

The data used for this study consist of HRSC images (Neukum and Jaumann, 2004), Mars Global Surveyor (MGS) Mars Observer Camera (MOC) images (Malin et al., 1998), Mars Reconnaissance Orbiter's (MRO) High Resolution Imaging System (HiRISE) images (McEwen et al., 2007), and Context camera (CTX) images (Malin et al., 2007). In particular, we used HRSC images #4310 and #7233, with nadir resolutions of 15 m.pixel^{-1} and 25 m.pixel^{-1}, respectively, for a thorough study of the morphology and geometry of the valleys and detailed mapping. Regional maps and mosaics in sinusoidal projection are centered at 325°E longitude.

We used two triplets of HRSC images acquired on orbit #4310 and orbit #7233 to generate two HRSC DEMs (Digital Elevation Models) using the DLR Berlin tools developed for the Mars Express mission (Scholten et al., 2005; Gwinner et al., 2007) and successfully applied to martian valley networks (Ansan et al., 2008, Mangold et al., 2008). Each image triplet consists of a nadir and two stereo images. The altimetric points extracted from these triplets have been projected onto the Mars datum (Duxbury et al., 2002) using a sinusoidal projection at a spatial gridding of 60 m. A total of 2601473 tie points were detected on whole area covered by the image triplet #7233, using 3D coordinates that have a spatial accuracy of σ_x=8.3 m, σ_y=6.0 m and σ_z=5.5 m, implying a statistical height error of ~7 m for each point. A total of 7995029 tie points were detected on the area covered by the image triplet #4310, using 3D coordinates that have a spatial accuracy of σ_x=12.8 m, σ_y=9.5 m and σ_z=8 m, implying a statistical height error of ~10 m for each point. Regional topography was analyzed using the 1/128 degree Mars Observer Laser Altimeter (MOLA) gridded data (Smith et al., 1999).

A hydrologic analysis system, DNR hydromod, included in ArcView GIS (Loesch, 2001), was used to extract valley networks automatically from the DEMs. Automatic detection is mainly used for comparison between datasets, rather than as an independent valley-mapping technique. The automatic detection of valleys in DEMs always requires visual checking to confirm the presence of valleys in the images. The DNR hydromod algorithm has three steps: (1) the original topography (DEM) is modified, removing sinks to produce a continuous flow direction grid. This step is very important because sinks like pits or impact craters disrupt the drainage topography; (2) a flow direction grid is calculated where the steepest downslope direction is recognized from each cell to the eight neighboring cells (D8 algorithm); and (3) a flow accumulation grid is generated as the cumulative number of cells flowing into each downslope cell. Cells that have high flow accumulation may be used to

identify stream channels. This software therefore permits one to deduce the probable location of past stream flow based on the current topography.

Craters for chronology were counted and measured in a geographic information system (GIS) using sinusoidal projection. Crater statistics used isochrons developed for Mars (Hartmann and Neukum, 2001) and isochron-fitting tools developed by Michael and Neukum (2010).

3. Identification, mapping and stratigraphy of Holden ejecta

3.1 Ejecta blanket boundaries

Detailed mapping of Holden ejecta was done for the region north and west of Holden, where Eberswalde crater is located (Fig. 2). Grooves, rays, terminal lobes and megabreccias formed by the cratering process were used to determine Holden ejecta boundaries. Megabreccias contain coarse blocks of varied size, shape and composition that are ejected by impacts. They are distinguished from coarse-grained sediments by their lack of organization and poor sorting. Megabreccias are frequently observed in central peaks and ejecta of large craters on Mars (Mc Ewen et al., 2007, 2009, Grant et al., 2008). Although a map of Holden ejecta was produced using Viking data (Grant 1987), higher resolution data permit a more detailed map to be compiled. Many breccia blocks surrounding Holden are visible in lower resolution images such as CTX and MOC (Fig.3). Only two HiRISE images show blocks at a higher resolution, and in color. Blocks are frequently lighter-toned than the surrounding matrix, allowing clear identification (Fig. 3). Size is highly variable from the limit of resolution to a maximum diameter of 100 m. Shape is variable from angular to rounded. Local outcrops inside Eberswalde depression display blocks locally >10 m (Fig. 3g), which

are likely too large to have been deposited by superimposed channel deposits. In color images, breccia blocks display various colors, as, for instance, in Fig. 3j where three blocks display three different colors. This suggests compositional diversity, as expected for crater ejecta. Breccias are found all around Holden, likely because they correspond to Holden impact ejecta. Given this extensive coverage centered on Holden crater, it is unlikely that all these breccia would correspond to smaller crater ejecta or local sedimentary breccia. South of Holden, terrains are more homogeneous and breccias are much more difficult to identify, likely due to the presence of the mid-latitude ice-bearing mantle that exists poleward of 25° in the southern hemisphere (e.g., Mustard et al., 2001).

In addition to breccia, grooves and rays within the ejecta blanket are detected by identifying lineations radial to Holden's center (Fig. 2). Terminal lobes are often difficult to identify around large craters compared to mid-sized craters with well-developed lobate ejecta (Carr et al., 1977, Mouginis-Mark, 1987, Costard, 1989, Barlow, 1990, 1994, Baratoux et al., 2002, 2005). The boundary between continuous ejecta and discontinuous ejecta in Figure 2 is identified by the increase in secondaries (and rays formed by secondaries) compared to sparse or inexistent secondaries where breccias are well identified (Fig. 3). This transition occurs 70-100 km beyond Holden's rim (2-2.5 crater radii R from Holden's center). Smaller craters on Mars (10 to 100 km in diameter) can have ejecta blankets extending more than 3R from the center (Barlow, 1994). Empirical relations from lunar data indicate an average extent of the continuous ejecta blanket of 2.3R±0.5R for a crater of Holden's diameter (Melosh, 1989). A continuous ejecta blanket extending 2R to 2.5R from the crater rim is therefore consistent with our knowledge of how craters form. The Eberswalde sedimentary deposits and associated feeder channels are within 2R of Holden, so are likely within the continuous ejecta blanket of Holden (Fig. 2).

3.2 Crosscutting relationships between Holden ejecta and Eberswalde valleys

Figs. 3 and 4 show three close-ups of MOC and HiRISE images along the main tributary leading to the Eberswalde fan. The valley is filled by aeolian material distributed in transverse ripples and dunes that hide bedrock. The valley sides expose cohesive bedrock containing blocks that are several meters to several tens of meters wide and usually lighter-toned than the finer material surrounding them, indicating this valley is incised into brecciated bedrock. This breccia is similar to that observed all around Holden's northern rim, and is mapped as part of the Holden continuous ejecta blanket. At the location of Figure 4c, the valley depth reaches 150 m (MOLA data) with the breccia exposed along the entire wall of the scarp. This gives a sense of the volume of material in the continuous ejecta blanket near the location of the valley outlet, just 50 km north of the Holden rim.

Empirical scaling laws for ejecta thickness estimated from explosion experiments and from lunar data express the ejecta blanket thickness H as a power law decaying with distance from the crater center r as (Mc Getchin et al., 1973):

$$H=0.14R^{0.74}\,(r/R)^{-3} \qquad (1)$$

This relation was preferred to Martian empirical laws (e.g., Garvin and Frawley, 1998) that used craters more or less degraded by glacial and atmospheric activity in the northern plains. Using equation (1), we find the expected ejecta thickness for a 75 km radius crater would be ~125 m at 50 km from the rim (as in Figure 4c). This thickness is consistent with our local interpretation of the location of continuous ejecta suggesting post-Holden erosion was insufficient to remove much material from the ejecta blanket, except by individual valley incision. Note that the thickness decreases strongly with increasing distance from Holden's rim: the relation predicts a decrease from ~240 m at 25 km from the rim to ~70 m at 75 km from the rim (2R).

3.3 Crosscutting relationships between Holden ejecta and other fluvial valleys

Holden secondaries can be observed >300 km from Holden's rim (Fig. 2). Secondaries are usually identifiable as butterfly-shaped and elongated craters, frequently with small crater chains. If elongated, their long axis is always radial to Holden center. Several examples show that Holden secondaries overprint valley networks. This is visible 150 to 300 km north of Holden where well-developed valley networks are crosscut by a crater chain (Fig. 5a). These networks do not connect with valleys breaching Eberswalde crater. Just south of this example, Arda Valles are also superposed by a few elliptical craters: two of these are 2 km across (minor axis) (Fig. 5b). None of these secondaries display obvious erosion by fluvial activity or other indicators of reactivation of the fluvial valleys after these small impacts formed. If fluvial activity occurred in Arda Valles after these secondaries, it must have been limited in amplitude to explain the overall lack of late incision. The geomorphic style of deeply incised and regionally integrated incision of Arda Valles and the valleys north to them is comparable to classical highland valley networks that are dated as Late Noachian - Earliest Hesperian (e.g. Fassett and Head, 2008).

To the north-east of Holden, Ladon Vallis is a ~40-50 km wide channel that is part of the Uzboi-Ladon-Morava (ULM) system of outflow channels that may have connected Argyre to Chryse Planitia (Grant and Parker, 2002). A secondary crater chain is superposed on terraces of Ladon Vallis (Fig. 5c). Ladon Vallis is suspected to be Late Noachian - Early Hesperian (Grant and Parker, 2002), possibly extending later well into the Hesperian (e.g., Grant et al., 2008). Thus, the crosscutting relationship between Holden secondaries and Ladon Vallis would imply an even younger age for Holden crater than the two previous examples with valley networks.

4. Chronology from crater densities

Crosscutting relationships show that Holden ejecta postdate most Late Noachian valley networks, but predate those leading to Eberwalde depositional fans. Dating the Holden impact more precisely would then constrain the absolute timing of these processes - in particular, a maximum age for Eberswalde fluvial and lacustrine activity. Crater counts were carried out on the northern ejecta blanket and on the interior of Holden (Fig. 6). For the northern ejecta blanket, the area on which craters are counted corresponds approximately to the area of the continuous ejecta blanket as mapped in Figure 2. A slightly larger area was used for counting craters inside Holden (Fig. 6), where only craters >1 km were counted in order to limit crater removal due to resurfacing by sedimentary filling.

First, we can use the Tanaka method (Tanaka, 1986, Werner and Tanaka, 2011) to determine epochs from the cumulative number of craters of more than 1 and 2 km, i.e. N(1) and N(2). The N(5) would be vulnerable to Poisson noise because of the low number of craters. We obtain N(2)=382±171 craters/10^6km^2 for the ejecta blanket and N(2)=610±184 craters/10^6km^2 for the interior of Holden. Uncertainties are large because of the low number of craters, but the estimates overlap for N(2) in the range 450 and 550 craters/10^6km^2. This N(2) corresponds to a Late Hesperian age based on the stratigraphy of Werner and Tanaka (2011) (Table 1). Even assuming the N(2) of Holden's interior is more reliable because of the greater number of craters, the age found is shortly after the Early-Late Hesperian boundary.

The new stratigraphy proposed by Werner and Tanaka (2011) also enables us to use the frequency of craters >1 km diameter for dating. With 25 craters >1 km for Holden ejecta we obtain N(1) = 1913±383 craters/10^6km^2 and with 23 craters on Holden's floor we obtain N(1)=1277±266 craters/10^6km^2 for Holden interior. In contrast to the N(2), the latter value is now lower than that of ejecta, which may be a result of the stronger modification by eolian blanketing on Holden's floor. According to this new timescale, the N(1) found for the ejecta of 1913±383 craters/10^6km^2 is close to the Late Hesperian/Early Amazonian boundary, and more consistent with an Early Amazonian age than a Late Hesperian age.

Applying Hartmann incremental plots (Hartmann and Neukum, 2001) to the ejecta blanket, the graphical age is found to be 3.2-3.4 Gy (Late Hesperian) considering only bins from 700 m to 5 km diameter (Fig. 6). Craters <700 m are undercounted due to erosion and infilling, explaining the shift to younger ages for this size bin (Fig. 6). Craters >2km are rare and suffer from Poisson noise. The largest craters in Holden interior are slightly overabundant (but with large error bars) relative to the isochron defined by smaller craters. To calculate Holden's age, we exclude craters smaller than 1 km because of the major resurfacing inside Holden, and only use larger craters. The age of Holden crater using this technique is still consistent with an age slightly after the Early Hesperian - Late Hesperian boundary (~3.4 Gy in Hartmann scale, Tab. 1).

A similar trend is shown using a Neukum cumulative plot based on Ivanov's modeling (Ivanov, 2001, Michael and Neukum, 2010). Model ages of 3.45 Gy and 3.58 Gy are derived for ejecta and interior respectively, with standard deviation ~0.1 Gy (Fig. 6). Taking into account this error, these ages are consistent with an age of ~3.5 Gy, corresponding to a Late Hesperian age (Late/Hesperian boundary at 3.65 Gy in this model, see Table 1). Given uncertainties in these models as well as limitations due to small crater degradation, an age inside the Early Hesperian is not excluded.

Most ages for Holden crater found by the different methods used postdate the Early Hesperian - Late Hesperian boundary when translating these ages in Tanaka scale (Tab. 1). The youngest age indicates an age slightly postdating the Late Hesperian - Early Amazonian boundary. Therefore, crater counts favor a formation of Holden crater in the Hesperian period, probably in the Late Hesperian. Eberswalde fluvial activity postdating Holden crater is therefore also this age, or even younger. This chronology is consistent with crosscutting relationships that placed Holden crater after the formation of main valley networks and after the Early Hesperian outflow channel Ladon Vallis. It is also consistent with recent crater counts made on alluvial fans in southern Margaritifer Terra including the Holden bajadas, which show Late Hesperian and Early Amazonian ages (Grant and Wilson, 2011).

Determining whether or not Eberswalde fluvial activity occurred immediately after Holden impact is also important, especially for constraining possible links between the Holden impact and the Eberswalde fluvial activity. This requires finding, or not, a time gap between the two events, e.g. observing how many craters postdating Holden ejecta were cut by the fluvial activity later. This question is hard to resolve, even with high resolution imagery. We did not find a significant candidate population of small craters that definitively satisfy these conditions. For example, small craters truncated by valleys feeding into the main Eberswalde fan may have been affected by post-fluvial widening of the feeder valleys, not by the fluvial activity itself. A major problem is that aeolian infill and erosion occurring in the last 3 Gy has modified fluvial landforms and small craters in the Eberswalde region.

A 16 km diameter crater on the NW rim (Bigbee Crater, marked “X” in Fig. 3a) is a candidate as it seems to impact Holden rims, and is eroded by Holden rim retreat associated with the deposition of the Holden bajada. As illustrated by the example of Ardas Valles (pre-Holden) and the valleys sourcing the small fans in North Eberswalde, it is possible for spatially adjacent watersheds to be fluvially active at different times. In this case, fluvial activity at Holden could immediately postdate the Holden impact, but the Holden bajada would form (perhaps by a different mechanism) after a time gap. In addition, this crater when plotted on the crater count population (Fig. 6a, in red) appears out of the count like if its presence was statistically unlikely. No smaller craters exist that seem fluvially eroded in the same way as it should be the case in a statistical crater distribution. Thus, the fact that it is the single crater eroded like this questions its chronological relationship with Holden. For example, Bigbee may be an old crater not fully modified by Holden impact, explaining its shallow and non-circular shape, especially on its southern rim that is almost fully eroded. Lunar examples include the 180km-diameter Crater Tsiolkovskiy (20.1°S, 129.1°E, for example on the Apollo view AS15-M-0757), which has incompletely blanketed 20-30km diameter craters on its NE rim showing it is possible to partially preserve craters of the size of Bigbee so close to large craters. As a last alternative, Bigbee’s formation could have been coeval to Holden. Indeed, recent studies show that binary asteroids represent 1/6 of >300 m

large body among near earth asteroids (e.g., Pravec et al., 2006, Pravec et al., 2012). Observations at Venus surface confirm the accuracy of these estimations (Cook et al., 2003). Any moon must orbit well within the Hill sphere of the primary asteroid (Murray & Dermott, 2000). The Hill sphere radius is $R\_Hill = a * (m/M)^{1/3}$ where a is semimajor axis of Mars, m is asteroid mass, and M is the solar mass (Murray & Dermott, 2000). Suppose the Holden impactor was 15 km diameter (typically 1/10 to 1/20 of the crater final diameter), with density 3000 kg/m^3. The Hill sphere radius at Mars' orbit is then 3,000km and can comfortably accommodate the ~km-sized Bigbee impactor. To solve the question of a time gap in future studies, a population of small craters predating and postdating should be identified to avoid poor statistics due to a unique impact. A systematic survey of small craters at Holden's rim at HiRISE scale may give a beginning of an answer.

Rice et al. (2011) interpret lineations within Eberswalde Crater as faults due to regional tectonic activity, which would imply a time gap between floor deposits interpreted as Holden ejecta and lacustrine sediments on the Eberswalde floor. These lineations are interpreted in our study as part of the ejecta grooves surrounding Holden. Indeed, these lineations trend NNE inside Eberswalde, which corresponds to a direction radial to Holden crater. This NNE trend is not found outside Eberswalde, whereas additional lineations are found with other trends, always radial to Holden crater center, supporting the impact-groove interpretation. The interpretations of these lineations as faults may come from subsequent displacements along pre-existing scarps due to differential compaction under sediment (or ejecta) overburden; something frequently observed in terrestrial basins (e.g., Freeth and Ladipo, 1986). In addition, radial impact-related faults have been identified on Earth (e.g., Koeberl and Henkel, 2005).The fault and ejecta groove hypotheses are therefore not mutually exclusive. In our assessment, faults would not be related to any Tharsis stress as hypothesized by Rice et al. (2011), but local to the Holden region, and, in such a context, the identification of a non-negligible time gap between ejecta and sediments deposition is non-unique.

5. Eberswalde basin and valley morphology and dynamics

Given the cross-cutting relationships from Section 4, which indicate that the Eberswalde fan formed after the Holden impact, the analysis below uses watershed geometry and valley morphology to constrain processes. These observations are not exhaustive: their goal is to highlight a few characteristics that can be used in modeling of the sediment infill, to examine the rates and processes of deposition, and later in the discussion of climatic versus impact triggers for fluvial activity at Eberswalde.

5.1 Watershed analysis

We compare valley networks in the Eberswalde catchment as observed in the HRSC images, and as automatically detected by DNR hydromod (see section 2). The Holden northern outer rim is incised by numerous valleys (Fig. 7). Several valleys interconnect to form a branching pattern debouching into Eberswalde crater and terminating in the fan. Nevertheless, some valleys are not linked to this pattern, despite being part of the same watershed. They are discontinuous, lack connection with downstream tributaries, and usually vanish suddenly. The valley network is also asymmetric: Valley heads are more numerous in the southern section while large parts of the west and north of the basin are devoid of any valleys despite having similar slopes and drainage areas. This does not seem to be an issue of image resolution because a similar asymmetry was observed in higher resolution datasets such as CTX and MOC.

The area defined by all the mapped valleys is ~5 000 km^2. Based on both HRSC and MOLA topography, the watershed appears to cover a wider area than do the valley networks. The watershed covers an area of ~12,700 km^2. The abrupt end of the watershed to the western edge of the geographic box is partly due to the DEM limits, but the true limit does not

extend much more to the west (~30 km) as seen on the MOLA DEM. Automatically detected valley segments crosscut current topographic lows without any corresponding evidence for incision in the HRSC images. A similar result is observed from MOLA data, despite the lower density of the calculated network from this dataset (Fig. 7f). These results show that the visible valley network did not cover the whole topographic watershed. The fact that valleys developed in the lower eastern section of the watershed only, and not in the western upper section, could result from (i) high rates of infiltration into the subsurface, possibly due to the presence of Holden ejecta; (ii) a geologically brief period of fluvial activity; (iii) an irregular input of water in the watershed, such as that suggested by the asymmetry in valley heads, or a combination of these effects; (iv) upper catchment dominated by overland sheet flows until slope was significant enough to focus into valleys; (v) supraglacial flow in the upper catchment transitioning to bedrock incision in the lower parts of the catchment.

5.2 Boulders in the inverted channels of the depositional fan

The geomorphology of Eberswalde's fan has been studied in detail (e.g., Lewis and Aharonson, 2006, Pondrelli et al., 2008, 2011, Rice et al., 2011). All studies interpret topographic high-standing ridges as inverted channels created by differential erosion. These channels display sinuous and accretionary shapes, usually interpreted as meanders (Malin and Edgett, 2003). HiRISE images show some of these inverted channels contain meter-scale blocks (Howard et al., 2007, Pondrelli et al., 2008). The presence of boulders in the quiet depositional environment of a fan is intriguing because on Earth fan deltas are usually dominated by silt and sand-sized deposits, sometimes gravels (Colella and Prior 1990), but not boulders.

Images show that boulders are up to 2 m in size (Fig. 8). They could have formed by weathering of chemically cemented layers and, in this case, would not be relevant to understanding the primary depositional environment. However, deposits with boulders are

strictly limited to well-defined blocky layers separated by non-blocky layers (Fig. 8d). Sometimes the layering shows alternation of competent blocky layers and finer grained layers (Fig. 8b, see also Fig. 15c in Pondrelli et al., 2008). 20 m spaced polygons affect the finer deposits much more easily than the blocky deposits (Fig. 8d) also suggesting a difference in grain size between the two types of layers. The sharp confinement of boulder deposits to individual layers (as in Figure 8b, c or d) argues that boulders were fluvially transported because chemical induration often occurs regardless of the layering. In addition, it appears that these sinuous channel deposits have been inverted by erosion because of the presence of boulder-bearing deposits in the uppermost part, perhaps because those layers are more resistant to erosion.

The inference that these boulders were deposited in the channel floor has implications for the channel dynamics. Howard et al (2007) proposed that the boulders could be transported by normal fluvial flows if the bed material were strongly bimodal, with a dominant sand or fine gravel bed with a minority of coarse boulders. Nevertheless, some layers seem to be very boulder-rich (Fig. 8), casting doubt on the idea that they are only a minor component. In addition, Kuhnle (1993) argues that when the sediment has a strongly bimodal size distribution, but uniform density, the shear stress to transport boulders is the same as it would be for sediment composed entirely of boulders. Under such high shear stress the rest of the sediment would not remain deposited for long, but rapid erosion would begin even when conditions for the blocks are favorable for deposition (Kleinhans and van Rijn, 2002, Kraal et al., 2008b).

One solution to this problem is that the flows were dense enough to transport boulders. Dense flows might occur due to dam breaking, sudden aquifers discharge, or flash floods. Dam breaking is a possibility due to the observation of an upper depositional area, before the entry to the canyon that sources the Eberswalde fan (immediately south of the location of figure 4b). The observations of multiple beds with boulders at different levels of the deposits would require multiple dams and breaches during the whole fan formation,

something uncertain given the lack of observations such as multiple terraces, for example, that could confirm such hypothesis. Several wide valley heads could also be interpreted as having been generated by small outflows. Dense flows are discussed in the modeling below.

A second alternative is that boulders have a low density. Indeed, Holden ejecta would constitute a huge source of blocks of very diverse size and density. Thus, blocks in channel deposits can correspond to individual blocks of impact breccia present upstream inside the Holden ejecta and transported downstream. Ejecta in such huge impacts can be heated enough to be melted partially or totally, which can create more porous blocks similar to volcanic pyroclastic rocks or lapillis (e.g. Melosh, 1989). For example, individual blocks of breccias collected by Apollo missions are between 15% and 25% of porosity (Macke et al., 2011), therefore decreasing their average density. Block entrainment is strongly sensitive to block density (Kleinhans and van Rijn, 2002). A decrease by ¼ in density of only parts of the Holden breccia blocks could explain why block entrainment can occur more easily in Eberswalde fan than in other locations. In any cases, if interpreted as transported boulders and not as weathering products, the presence of these boulder-bearing channel deposits require specific conditions including high discharge rates, in the range of 500-1000 $m^3.s^{-1}$ (for rock density 2650 $kg.m^{-3}$) as calculated by Howard et al., 2007, light density of blocks, dense flows to transport blocks, or a combination of these properties.

5.3 Channel dynamics and sedimentary body growth

By modeling the sediment deposition, it is possible to broadly constrain the rate and formation time-scale of delta features on Mars (Kraal et al. 2008b, Kleinhans et al., 2010). The general model presented in Kleinhans et al., 2010 calculates the growth of a sedimentary body in a crater lake, represented by a low-gradient, subaerial cone on top of a high-gradient, subaqueous cone. The volume of the cone is constrained by the influx of sediment while the elevation of the break in slope, i.e. the shoreline, is constrained by the

453 influx of water. The parameters that determine which morphology emerges are the supply of
454 sediment and water to the basin, the size of the basin and the duration of the flow (Kleinhans
455 et al., 2010). The water and sediment fluxes were calculated with physics-based predictors
456 based on the feeder channel dimensions and gradient.

457 The dilute scenario (Fig. 9, left) represents sediment transported by a fluvial flow with
458 predominantly liquid water. Duration of accumulation to form a deposit with size and shape of
459 the Eberswalde fan would be two decades. The dense flow scenario (Fig. 9, right) represents
460 the dense debris flow scenario, i.e. not a dilute flow but a slurry. This scenario forms the
461 deposit in less than two weeks. The total flux of water and sediment in the dilute and dense
462 cases are exactly equal at 8.7×10^4 m^3/s. In the dilute case, the flow had 0.05% (Solid:Water
463 ratio S:W=0.0005) sediment concentration by volume calculated from a semi-empirical
464 sediment transport predictor for gravel bed rivers, and in the dense case the flow had an
465 imposed 30% (S:W=0.3) sediment concentration by volume. Here the dense flow is taken as
466 really dense (S:W=0.3), but flows can be defined as dense for S:W as low as 0.01. Assumed
467 feeder channel dimensions for the dilute case were 500 m wide, 25 m deep at a gradient of
468 0.034 with a representative (median) gravel particle diameter of 0.1 m.

469 The dilute scenario requires the Eberswalde crater to overflow at about 250 m above
470 the existing fan surface. Observations however, do not show the presence of any overflow,
471 and, on the contrary suggest a relative stable lake level, as shown, for instance, by the main
472 fan upper surface, not incised by subsequent episodes. If the crater had no overflow, then
473 the fluvial flow discharge required to transport the sediment contained in the fan would have
474 filled up the crater to a much higher level than can be accounted for by the elevation of the
475 most distal deposits of the fan, whilst the sediment would be deposited as a thin drape on the
476 crater wall rather than a long delta (Kleinhans et al., 2010). This is because typical sediment
477 concentrations in dilute fluvial channels are 10^{-3} to 10^{-4}. The condition of a constant overflow
478 height for the dilute case is therefore essential. If overflow height varied even slightly, one

would expect to see delta lobes at very different elevations and perhaps incised delta lobes as well. Neither are observed.

Two possible alternatives exist to stabilize lake level: infiltration or evaporation. Infiltration into a permeable crater floor may have occurred, aided by the high permeability of ejecta deposits. However, infiltration reduces as the subsoil is increasingly saturated. It would be an unlikely coincidence for the waning infiltration permeability of the crater floor to be exactly matched by a waning flow discharge or a series of discharge pulses, and this would have dramatically reduced sediment transport capacity anyway. Results of the dilute flow modeling predicts that more than half of the fan consists of steep foreset deposits at the angle of repose, but steep foresets appear to be rare or absent (e.g., Lewis and Aharonson, 2006). The second alternative is a rapid evaporation rate compensating the lake infill. However, here too, the evaporation must match the inflow of liquid water, but there is no obvious mechanism to adjust evaporation rates to balance discharge at Eberswalde. Energy available from insolation would limit evaporation from the lake to 0.1 – 1 m/yr (R. P. Irwin III, submitted manuscript), a value insufficient to compensate influx in the dilute model. Overall, this scenario seems impossible. There is a missing water sink.

The dense flow scenario (Fig. 9, right) does not require an overflow and produces mostly subhorizontal strata. The dense flow has about one-third of sediment, and two-thirds of water. This means that the water level in the crater does not rise fast, and the deposit can prograde far into the crater. The minimum formation time for the deposit is estimated at only a few days, but such a large fan is more likely built up from several flow events, perhaps coupled to seasonality, damming, or surges, so that years or decades formative time are equally likely. Such a dense flow could also explain the presence of the large boulders. Possible weaknesses of this model are that (1) a trigger is required to cause a dense flow that is self-maintained (Kleinhans et al., 2005), and (2) that it may be more difficult to explain the sinuosity of the few meanders observed. Note, nevertheless, that meander formation has

been debated on Earth for hyperconcentrated flows in China (Xu, 2002, van Maren et al., 2007, van Maren, 2009).

Overall, dense flows match more observations at Eberswalde than do dilute flows, but do not provide a definitive solution. Only a subset of possible parameter combinations has been explored, and an intermediate solution may explain better observations. Nevertheless, the main lesson from this modeling is that water influx from a dilute channel should increase the water level, contrary to observations of a nearly constant level, and that a dense flow may solve this issue.

6. A climatic origin for Eberswalde fluvial activity in the Hesperian?

6.1 Implications of the chronology

The estimated age of Eberswalde watershed and lacustrine activity - post-dating Holden crater, probably in the Late Hesperian - raises the question of the origin of the liquid water. Fluvial activity is known to have peaked during the Late Noachian and Early Hesperian (e.g. Carr, 1996, Hynek and Phillips, 2001, Craddock and Howard, 2002, Fassett and Head, 2008). Younger fluvial activity has been observed at different locations of the planet, either as local fluvial and lacustrine process in post-Noachian regions such as Valles Marineris and Tharsis region (Mangold et al., 2004, Quantin et al., 2005, Mangold and Ansan, 2006, Mangold et al., 2008), in Newton/Gorgonum (Moore and Howard, 2011), in Xanthe terra (Warner et al., 2010a), several volcanoes (Gulick et al., 1990), local mid-latitude ejecta blankets (Mangold, 2012), and craters with alluvial fans (Grant and Wilson, 2011), or as local reactivation of ancient valley networks (Baker and Parkridge, 1986, Ansan and Mangold, 2006, Bouley et al., 2009, 2010). Nevertheless, the erosion rate has strongly decreased from a relatively high erosion rate in the Noachian to a very low one in the Late

Hesperian (Craddock, et al., 1997, 2002, Golombek et al., 2006) suggesting the global climate had already cooled/dried by the Late Hesperian. The good preservation of Holden ejecta, as well as its secondaries, indicates limited erosion rate after its formation, and a correspondingly low rate of fluvial activity compared to more strongly degraded Noachian craters.

Whereas fluvial erosion declined in the Hesperian, glacial activity is recognized to have dominated Amazonian mid-latitudes. The mid-latitudes of Mars feature distinctive landforms, including ice-bearing mantling deposits and periglacial landforms (e.g., Squyres and Carr, 1986, Mustard et al., 2001, Mangold and Allemand, 2001, Mangold, 2003, Byrne et al., 2009, Levy et al., 2009, Hauber et al., 2011) and gullies on steep slopes (e.g., Malin and Egdett, 2001, Costard et al., 2002, Balme et al., 2006, Mangold et al., 2010). Recently, sparse, shallowly incised, fresh-appearing valleys were discovered using new imaging data (e.g. Fassett et al., 2010, Howard and Moore, 2011). In Newton Crater and in Gorgonum basin the valleys were formed at about the Hesperian to Amazonian transition (Howard and Moore, 2011), slightly later than Holden formation. These mid-latitude valleys are distinct from the older, late Noachian valley systems which are deeply dissected, and are generally of much larger spatial extent (e.g. Craddock and Howard, 2002, Howard et al., 2005, Irwin et al., 2005, Ansan et al., 2008). An episodic formation has been proposed for these late-stage valleys. For example, outflow channels formed during Late Hesperian are known to have released a significant amount of water, increasing the atmospheric water vapor pressure (Baker et al., 1991) and possibly triggering Late Hesperian valley networks in Valles Marineris region (Mangold et al., 2008). The Late Hesperian was therefore an epoch during which fluvial activity existed, but was limited to regional occurrences, with a limited amount of erosion, and probably with mean annual temperatures below freezing.

6.2 Hypotheses for a climatic origin

559 A consequence of dating the fluvial landforms to the Hesperian is that the climate
560 under which they formed may be cold and dry, possibly as dry as the present day. The fluvial
561 activity at Eberswalde could have occurred due to transient climatic episodes. Transient wet,
562 possibly warm, climate episodes could involve (1) episodic melting of snow and ice either
563 during optimal orbital conditions, (2) intensive volcanism releasing greenhouse gases, (3) a
564 brief episode of global warming from a large impact somewhere on Mars, (4) reduction of
565 snow albedo by dark fine-grained impact ejecta or ash, or (5) water release from the outflow
566 channels in the Xanthe Terra region (Baker et al., 1991; Segura et al., 2002, Howard and
567 Moore, 2011, Kite et al., 2011a, Grant and Wilson, 2011). The presence of the mid-latitude
568 mantle immediately south of Holden suggests that snow deposition was common at these
569 latitudes. Episodic snowmelt subsequently to snow deposition is also possible from local
570 conditions. Lakes inside Holden (Grant et al., 2008), and also inside Uzboi Vallis south of
571 Holden (Grant et al., 2011), if they had some open water, could have generated localized
572 snowstorms as proposed for regional fluvial activity elsewhere on Mars (e.g. Juventae
573 Chasma, Kite et al., 2011a, b). In such a climatic hypothesis, the limited extent of valleys in
574 Holden ejecta would be explained by considerable infiltration into ejecta and resultant
575 downslope emergence of water as runoff at lower elevation.
576
577 In such a cold climate, Eberswalde lake surface would quickly freeze, possibly even
578 during fluvial infilling. Ice along the shoreline can be a very effective geomorphic agent. For
579 example, on Earth, broken ice can be blown by the wind toward the shore, where it can
580 gouge sediment and raft it up over the shorelines in a processes called ice push (for an
581 overview see Reimnitz, et al 1990). In terrestrial lakes and arctic seas, ice push can destroy
582 previously existing geomorphic features and drive sediment up to 400 m from the open water
583 shoreline (e. g. Mahoney et al 2004). These processes cause irregular shoreline features,
584 including shore ridges that vary in elevation (because the process is control by ice push by
585 wind, rather than surface wave action). Even permanently ice-covered lakes, such as ones
586 located in the McMurdo Dry Valleys that also contain deltas, have well-preserved shorelines

(Hall et al., 2010). Ice-cover in Eberswalde could have a dramatic effect on shoreline and fan geomorphology especially in the case of repeated freeze-thaw cycles or thin ice as would be predicted by the global climate change. However, shoreline formation and ice-push effects on Mars may be mitigated by the lower atmospheric pressure on Mars, which decreases the formation and size of wind-water waves (Lorenz et al. 2005). On Mars, Moore and Wilhelms (2001) proposed that features mapped within the Hellas Basin were best explained by ice-covered lake processes. Similar features, either strong evidence for open-water or ice-covered shorelines or ice-covered lake morphology as described in the Hellas Basin, have not been identified in the Eberswalde Basin yet.

A purely climatic origin of the Holden and Eberswalde system of valleys and fans could have occurred during relatively warm episodes within a globally cold climate. In this case, lacustrine activity in Eberswalde would be regarded as a transient episodic lacustrine activity representative of the latest aqueous processes in a cold climate. Any model for Eberswalde fan formation, including climatic hypotheses, should explain the following observations: (i) the lack of fluvial erosion on Holden secondaries suggests that the fluvial activity did not significantly affect the terrains north of Eberswalde crater; (ii) the apparent limited period of activity of the lake and fan formation questions why this activity was so restricted in time, instead of being reactivated several times during the past, as would be expected for quasi-periodic climatic episodes; (iii) a climatic episode should be able to explain the occurrence of relative dense flows suggested as a possibility by modeling and by the transport of meter-sized boulders into the river system, which may be a challenge with only limited runoff from snowmelt.

7. The role of Holden impact in Eberswalde fluvial activity

7.1 What mechanisms could link the Holden impact to fluvial activity?

We have shown that the presence of widespread ejecta of Holden in the whole watershed plays a role in the fluvial erosion: ejecta are a weak, possibly low-density material that is easy to erode compared to usual bedrock material and contains abundant boulder-sized breccia blocks. In this section, we speculate that the impact itself could have played a role in triggering fluvial activity. Impact craters have been invoked in Mars fluvial valley formation for decades (Brakenridge et al., 1985, Mouginis-Mark, 1987) but a definitive answer to this question has proved elusive, mainly because of the lack of supporting observations and detailed models quantifying the coupling between impact energy and fluvial runoff.

Mechanisms that could connect impacts to fluvial activity include: (1) long-term hydrothermalism in large craters that struck an ice-rich target (Brakenridge et al., 1985, Newsom et al., 1996, Abramov and Kring, 2005), (2) release of water from subsurface ice excavated by the crater as observed around Hale Crater (Jones et al., 2011), (3), short-term hydrothermal due to warm ejecta blanketing shallow ice, as observed for Sinton Crater which displays braided fluvial valleys on its ejecta (Morgan and Head, 2009), and observed in less spectacular fashion for >40 craters of 10-100 km in diameter located in the mid-latitudes (Mangold, 2012), (4) episodic snow deposition from climatic processes could melt if it lands on warm crater rims and ejecta, possibly explaining observations at Mojave Crater - Mojave displays unexplained but presumably impact-associated activity with well-developed gullies and depositional fans on its inner slope (Williams and Malin, 2008) - or (5) an impact into an ice-bearing crust that generates temporary climate modifications leading to precipitation if the impactor is big enough (Segura et al., 2002, 2008, Toon et al., 2010). All these processes require the existence of ice in the subsurface, or near the surface as snow/ground ice. Because of its position at 26° S, the Holden impactor may have struck ice-rich ground, as exists in the mid-latitudes today (e.g., Mangold et al., 2002). Mustard et al. (2001) concluded that the ice-bearing mantle is present in many locations south of -25°S of latitude in the southern hemisphere. More equatorial ground ice has also been detected in the outflow

640 channel region (Warner et al., 2010a, 2010b). Eberswalde crater is at the northern edge of
641 this mantle, and could have been covered by snow/ice in the past, especially if obliquity was
642 higher.

643

644 A 100 km diameter crater creates hydrothermal activity in the crater interior that can
645 last >100,000 years and can induce lake formation from groundwater (mechanisms (1) and
646 (2); Abramov and Kring, 2005). This process may explain prolonged fluvial activity on the
647 inner rims of large craters, (as is observed on the Holden rim), but not valleys observed on
648 ejecta from >50 km diameter craters where valley heads are observed far from crater rims.
649 Nevertheless, it is observed that many valley heads (Fig. 7) are located less than 30 km from
650 the rim of Holden, whereas there is a relative lack of valley heads far away from the crater
651 rim, suggesting that the proximity of Holden rim did provide favorable conditions for runoff.
652 Therefore, it seems possible that the heat produced by the impact and released at Holden
653 rims can contribute to melting ice present at this location. Warm groundwater seepage may
654 also explain the persistence of a lake in a freezing climate (Newsom, 2010).

655 Mechanism (3) requires the ejecta to be warm enough for melting water ice, such as a
656 shallow ice-rich mantle. Episodic deposition of snow on the warm crater (mechanism 4), or
657 the creation of snow from the impact-related water vapor release to the atmosphere
658 (mechanism 5), are other alternatives. The latter was proposed initially for impact basins
659 (Segura et al., 2002), but a 150 km diameter crater such as Holden might be sufficient to
660 trigger global climatic change (Segura et al., 2008). Regardless of whether or not the Holden
661 impact was sufficient to cause global climate change on Mars, Kite et al. (2011a, 2011b)
662 show that simulated lake sizes ~10^3 km^2 (smaller than Holden's crater floor area) are
663 sufficient to create a localized snowstorm in a cold/dry background climate that is continuous
664 as long as the lake surface remains unfrozen.

There are no good terrestrial analogs to the speed and scale of a basin-forming impact's hot ejecta curtain landing on icy target. Hot rock-snowpack interactions like those at Mount St. Helens are the closest Earth analogs (Pierson, 1997). In experiments with sand-sized grains and relatively low confining pressure, water vapor rising from the pyroclast-snow interface can fluidize pyroclasts, leading to rapid mixing and destructive lahars (Walder, 2000a, 2000b). Nevertheless, a greater confining pressure (as expected beneath the Holden ejecta layer) could suppress fluidization (Walder, 2000a, 2000b). A test of these various hypotheses can be difficult, especially for (4) and (5) which require climate modeling, which is beyond the scope of this paper. Mechanisms 1 to 3 require, at least, enough ice to enable melting to generate the water flux observed, enough heat for the water ice to melt, and enough time for the valleys to form. These points can be tested, as shown below.

7.2 Thermal effect of Holden impact ejecta

Large impacts form ejecta deposits around the crater that consist of a mixture of heated material and can be up to hundreds of meters thick. The Ries impact (Germany) shows ejecta breccia that experienced heating at >600°C (Engelhardt et al., 1994). In the case of Holden, the valleys cutting the ejecta show that 100-200 m of ejecta may have blanketed the surroundings including the entirety of the preexisting Eberswalde crater.

By calculating the thermal effect of such ejecta on the underlying ground, we are able to find the depth and time window within which a small amount of subsurface ice would melt. The heat flow equation is solved in a pure conductive case in 1D (e.g. Turcotte and Schubert, 1982):

$$-\frac{\partial}{\partial z}\left(\kappa\frac{\partial T}{\partial z}\right)=\frac{A}{\rho c}-\frac{\partial T}{\partial t} \quad (2)$$

where z is the 1D profile at depth, κ is the thermal diffusivity, *A* is the source of internal heat (radiogenic) ρ the volumetric mass, *c* the specific heat, *T* the temperature and *t* the time. Radiogenic heating is neglected, as is the geothermal gradient (low over <200 m depth) (see Mangold, 2012 for details).

Conservatively assuming 100 m ejecta initially at 300°C, melting could affect a vertical ground thickness of about 60 m within roughly 150 years. Assuming a temperature of 600°C, which is possible at least locally, a column thickness of 120 m of underlying ground would reach the melting point within roughly 300 years. Assuming thicker ejecta with a high temperature, as is possible 25 km north of Holden's rim (see section 3), a column thickness of 250 m of underlying ground reaches the melting point in 1200 years (Fig. 10).

These calculations provide an order of magnitude for the water release depth and time by this single process. Typical lifetimes of 100-1000 years from a 100-200 m thick subsurface layer are indicated (Fig. 10). Such durations seem to be compatible with observations based on previous studies and our fluvial modeling, despite using a different mechanism (Jerolmack et al., 2004) (Fig. 9). Thickness can be tested assuming a 5000 km^2 watershed (as a minimum from valley extent). The deposits in Eberswalde fan have a volume of 5 to 6 km^3 (Malin and Edgett, 2003) that would have required 60 km^3 of water assuming a sediment:water (S:W) volume ratio of 0.1. A 5000 km^2 basin could have generated approximately 500 km^3 of water if the first 100m was nearly-pure water ice, or 250 km^3 if this ice was contained in a 50% porous subsurface. Such a volume is 4 times more than the 60 km^3 predicted for a S:W of 0.1. A 4 times lower solid load (S:W of 0.025) seems possible. However, these estimates are upper bounds. Equation (2) does not consider the latent heat of melting, which may limit the water available for runoff. In addition, preserved valleys are widely spaced, so the channel network may not have efficiently drained the entire catchment.

7.3 Idealized models of post-impact runoff

715 In this sub-section, we assume that there was surface ice in the area of the Holden
716 impact. Holden ejecta would have produced runoff as it melted its way down into the ice. This
717 runoff could entrain sediment from the overlying ejecta. To explore the consequences for
718 Eberswalde hydrology, we solve an idealized 1D Stefan problem at each point in the
719 watershed, and sum the results (Alexiades, 1992). In the following model, we assume that
720 the surface ice layer is initially very thick, and has a uniform temperature (T_i = 210K) at the
721 time the ejecta begins to land. Our implementation has two steps. First, we use a 1D Stefan
722 model to generate a look-up table for melt rate as a function of initial ejecta blanket thickness
723 (H), initial ejecta blanket temperature (T_{ej}, assumed constant with depth), sediment:water
724 volume ratio of runoff (S:W), and time t. Second, we sum the 1D column output over the
725 Eberswalde catchment to find the watershed-integrated discharge, *Q*. Appendix B gives
726 details of our implementation.

727 Two robust results emerge from the integrated discharge model (Fig. 11): (1) Initially
728 there is a power-law decline in *Q* that can last <1 – 2 x 10^3 years, depending on parameter
729 choices, a timescale consistent with previous results (Fig. 10). The slope of the power-law
730 decline is always steeper than for any single column in the watershed. (2) Late-stage flow is
731 provided solely by the annuli close to the rim of Holden, which have the thickest ejecta. As
732 the temperature of this thickest ejecta temperature approaches the point where continued
733 melting cannot occur, catchment-integrated discharge shuts down exponentially.

734 We compared the output to constraints from Eberswalde morphology, finding that
735 more than enough water is produced by ejecta-melt runoff to fill the crater. The most difficult
736 constraints for an impact model to match are the need to avoid overflowing the top of the
737 Eberswalde fan, together with the requirement for large late-stage peak discharge to mobilize
738 boulders (see section 5). HRSC DTMs show that the volume of Eberswalde's fan is 5±1 km^3,
739 and the paleolake volume below an estimated paleolake level of -1400m is ~31km^3 (~66 km^3
740 below -1350m). Because there is no evidence for an exit breach from Eberswalde crater,
741 water could only have been removed through infiltration and sublimation/evaporation. As

742 noted in section 5, there is no evidence this model does not fit with a constant standing body
743 of water.

744 Infiltration is unlikely to accommodate more than 1 crater volume of Eberswalde in the
745 short time available. We find that if the ejecta temperature is as high as predicted by theory,
746 then far too much runoff reaches the main fan. This is true even if only 25% of the ice melted
747 reaches the main fan. To avoid flooding the delta entirely, it is necessary to reduce the ejecta
748 temperature to about 200°C (Fig. 11). If 100% of melt produced reaches the delta, this gives
749 a total melt production of 84 km^3, or 20 column meters averaged across the catchment (Fig.
750 11). This melt requirement is consistent with the thickness of regionally extensive past ice
751 deposits in the Southern mid-latitudes of Mars, which is inferred from pedestal crater heights
752 to have been ~40m (Meresse et al., 2006, Kadish et al., 2010).

753 To build a ~5-6 km^3 delta from an impact-triggered flow, a moderate dense flow (*S:W* >
754 0.06) is therefore required from our modeling. At the lower temperature, the model fails to
755 produce late-stage discharge that might be required to form the meanders by dilute late-
756 stage flow, but the meanders might have formed in weeks to months in the unconsolidated
757 material of a fresh dense flow deposit. In addition, if annual-average temperatures were
758 below freezing, melt would accumulate beneath ice dams and crusts. Discontinuous release
759 could produce a spectrum of ice-breakout floods (jökulhlaups) of varying sizes as discussed
760 in section 4.

761 We conclude that idealized models of Eberswalde catchment response to the Holden
762 impact can meet many, but not all, of the observational constraints at Eberswalde as
763 currently interpreted. If Eberswalde's fan was formed by post-impact runoff, this must have
764 been by a moderately dense flow. However, we have not thoroughly explored the parameter
765 space. For example, if the ejecta were hotter near the surface than at depth, as expected
766 theoretically because of stratigraphic inversion during excavation, this would lead to a more
767 gradual decay of the meltwater pulses.

768 Clear predictions from this model are: (i) Because of the 10^2 – 10^3 yr timescale for delta
769 formation, delta deposition should be roughly continuous, with little to no paleosol
770 development (except at the top of delta, and the present-day erosion surface). Multiple lobes
771 within Eberswalde's basin do not provide evidence for multiple phases of activity, because
772 multiple lobes can be produced experimentally under constant external forcing (Kim &
773 Jerolmack, 2008, Hoyal and Sheets, 2009). (ii) Monotonic decline of impact-induced
774 discharge should produce a fining-upward progression, possibly with debris flows at the
775 base. (iii) The basal fan sediments should be deposited immediately after Holden ejecta
776 lands in the Eberswalde basin, leading to low-temperature hydrothermal alteration of the
777 basal fan sediments. In any model, the exact nature of the sorting pattern of the deposits at
778 the grain size from micrometers to meters would certainly help to understand hydrology
779 better, but this would require *in situ* observations.

780

781 ### 7.4 Role of Eberswalde crater impact ejecta

782 In the chronology obtained from crater counts and stratigraphic relationships, Eberswalde
783 crater appears as an old crater strongly modified by fluvial activity (Malin and Edgett, 2003),
784 and so cannot contribute to the formation of the Eberswalde fan in the same way as Holden.
785 Nevertheless, this study shows that Eberswalde has undergone two periods of degradation:
786 A first period due to classical Noachian aged fluvial activity, from which no visible landforms
787 remain, but can be observed north of Eberswalde, and a second period after Holden ejecta
788 emplacement. Eberswalde crater has likely been eroded by previous valleys, which may
789 explain the presence of a well-defined watershed to the west of the crater (Fig. 7). Indeed,
790 fluvial valleys leading to Eberswalde may be better-developed there because of the pre-
791 existing shape of the topography before Holden formation.

792

793 ## 8. Discussion

794

795 8.1 Implications for the chronology of events in the Holden region

796 Whatever the origin of liquid water (atmospheric, near-surface or deep subsurface),
797 an important consequence of our findings is that the incision of most valleys takes place into
798 the ejecta of Holden, constraining relative timing. A summary of the Holden region
799 chronology from our study and past studies is shown in Figure 12.

800 During the Late Heavy Bombardment, in the Early Noachian, the "Holden basin" - a
801 larger and earlier impact that the "Holden crater" discussed along our study - and the Ladon
802 basin formed (Saunders, 1979, Schultz et al., 1982, Werner, 2009). These basins were filled
803 likely by sedimentary deposits as well volcanic flows during a period of active geologic
804 processes, including an enhanced hydrological cycle (e.g. Matsubara et al., 2011).
805 Eberswalde crater formed after these basins formed and were partially filled. Eberswalde
806 Crater's smooth shape and shallow depth suggests that it was also degraded by these early,
807 active infilling processes. Valley networks such as Arda Valles observed north of Holden
808 crater, but stratigraphically below distal Holden ejecta, formed at the end of this period, in the
809 late Noachian and beginning of the Early Hesperian (e.g., Fassett and Head, 2008).

810 Large outflow channels (Uzboï Vallis to the south of Holden, and Ladon Vallis to the
811 north of Holden) formed episodically in the Late Noachian/Early Hesperian (Grant and
812 Parker, 2002). All these landforms predate the formation of Holden ejecta. Holden ejecta are
813 superimposed on most fluvial landforms in the region, but not fluvial valleys leading to the
814 Eberswalde depositional fan. Valleys and fans draining into possible paleolakes in Erythraea
815 Fossa, immediately SE of Holden crater, also formed after the Holden impact (Buhler et al.,
816 2011). Uzboï Vallis has a late stage of activity which breached the southern rim of Holden
817 (Grant et al., 2008). There is no evidence that Uzboï Vallis was continuously filled by water
818 immediately before and after Holden, and distinct episodes are more consistent with the

episodic activity of these channels. Recent crater counts show crater retention ages for the Holden crater fans as late as Early Amazonian (Grant and Wilson, 2011).

8.2 Implications for Eberswalde sediment and bedrock composition

Whatever the trigger for fluvial activity at Eberswalde (global climate change, the Holden impact, or a combination), our results show that the incision of most Eberswalde valleys takes place into the ejecta of Holden. This observation has major implications for the composition of sediment delivered to the Eberswalde fan.

Eberswalde's main fan and crater floor contain phyllosilicates (smectites and chlorites), formed by alteration in an aqueous regime (Milliken and Bish, 2010, Rice et al., 2011). On Mars, most phyllosilicates are Noachian (Bibring et al., 2006, Loizeau et al., 2007, 2010, Mangold et al., 2007, Mustard et al., 2009). When clays are found in depositional fans, as in a number of locations on Mars (Ehlmann et al., 2008, Dehouck et al., 2010, Ansan et al., 2011) this may be because of *in situ* alteration due to long-term warmer/wetter climatic conditions, or fluvial erosion of clays out of older bedrock. If Eberswalde experienced short-term and late stage formation in the Hesperian, this would suggest that the phyllosilicates were transported to the fan, rather than being formed *in situ.* In that case, these minerals could correspond to phyllosilicates formed by hydrothermal alteration subsequent to the impact as observed on Earth (e.g. Muttik et al., 2010), suggested for Mars for decades (e.g., Newsom et al., 1980, Newsom et al., 1996, Newsom, 2010), and possibly observed in several craters on Mars (Marzo et al., 2009, Mangold et al., 2012a). Smectites and chlorites are frequently formed in suevite, as they formed at temperatures of 100-200°C - ejecta can maintain these temperatures for 10^1-10^4 years. Alternatively, impact excavation of blocks from the upper crust previously altered during the Noachian is also possible, such as from a pre-existing Holden-Ladon basin dating from the Early Noachian (Werner, 2009; Barnhart

and Nimmo, 2011). In either case, the alteration would not be caused by the short term fluvial activity or the lacustrine environment inferred at Eberswalde.

8.3 Holden impact effect versus climatic origin

Our stratigraphic constraints suggest that the Eberswalde fan formed in a climate interval much colder than originally suggested (e.g., Moore et al., 2003) . Studies elsewhere on Mars indicate that the Hesperian was a period during which water was usually frozen (e.g., Carr, 1996). Therefore, local transient forcing such as impacts should be considered alongside purely climatic processes as potential sources of meltwater. The latter hypotheses are possible for Eberswalde fluvial flows, but orbital variations such as obliquity changes are quasi-periodic, which is hard to reconcile with the inference of a single period of water activity in Eberswalde, unless this period was the last one. Volcanism, gas release during Xanthe Terra outflow channel formation, or late impacts might have altered the Hesperian climate.

As an example of climate modification by late impacts, the Holden impact itself likely triggered a variety of processes inside and around the crater that can explain several observations on its northern ejecta blanket. In section 7, ejecta warming and melting is shown to extend up to several 100s of years after impact. This is consistent with fluvial modeling, as shown in section 5 and Fig. 9. In these calculations, dense flows with S:W ratio of typically 0.02 to 0.3 are required to fit mass balance and energy balance constraints. Section 5.4 also suggests that dense flows might better explain observations of the main Eberswalde fan than the dilute flows that were favored in previous studies. Because of the rapid falloff of ejecta thickness with distance from the crater rim, the greater density of valley heads close to the Holden impact rim is consistent with a role for the impact ejecta in valley formation.

Neither the climatic nor the impact-trigger hypothesis can straightforwardly explain the nearly stable lake level. The presence of highly erodible fractured bedrock (impact breccia), possibly with lower density, can explain more rapid incision of valleys in the Eberswalde catchment than in locations with intact bedrock. For valleys draining into Eberswalde, this would imply higher incision rate, shorter duration of formation and presence of breccia blocks as well as easily transportable fine grain material. Breccia can also have a high infiltration rate. Therefore, Holden impact would have played a role in the formation of the Eberswalde crater fluvial system, at minimum from the accumulation of porous breccia.

Mechanisms that couple impact and climatic triggers for fluvial activity at Eberswalde are also possible (Segura et al., 2008). Hydrothermal activity associated with Holden-sized impacts can warm the ground for > 100,000 years, with decreasing amplitude from crater rims to external ejecta (Abramov and Kring, 2005). A crater lake is inferred inside Holden crater from the characteristics of layered deposits on Holden's floor (Grant et al., 2008). A lake in Holden could have generated regional high water vapor concentrations and other atmospheric changes favorable for precipitation. Weather systems driven by transient lakes have been modeled by Kite et al. (2011b) for the case of the outflow channel source region Juventae Chasma. In this hypothesis (no. 5 in section 7.1), the Holden impact could be the immediate cause of climate change, or be the passive host for a longer-lived lake. Future modeling may determine if this hypothesis fits the data better than the modeling of ejecta warming in section 7. For example, energetic constraints limit sunlight-driven snow-melt or ice-melt rate to 2-3 mm/hr on Early Mars (Kite et al., 2011a). No such limit exists for impact-triggered runoff.

Initially, Eberswalde was taken as a well-preserved example of many Noachian fans. With the younger age found, a question could be: Why does the Eberswalde fan appear to be unique when compared to other landforms of the same epoch? This applies to both hypotheses; i.e. globally warmer climate or impact-related melting, because impacts have continued subsequently to Holden, and because a globally warmer climate should not have

regionally-limited effects. Assuming an impact-related formation, part of the explanation may come from the uniqueness of the regional topography: A large crater (Holden) close to a pre-existing basin (Eberswalde) favorable to convergent drainage. We can also speculate that this uniqueness can be understood if Eberswalde-type fluvial deposits can only form when a Holden-sized crater strikes a fairly thick ice sheet. Kadish et al. (2010) measure low-latitude pedestal thickness at 114±53m. If the pedestals correspond to a single paleo-ice sheet of uniform thickness, then ~18% of the planet is covered with surface ice during low-latitude glaciations (taking the modern surface ice reservoir of $2.9\pm0.3 \times 10^6$ km^3 (Selvans et al., 2010; Plaut et al., 2007), and assuming small loss of water to space since Eberswalde formed). Assume low-latitude glaciations occur ~1/2 of the time (Laskar, 2004). Then priming conditions for low-latitude impact-triggered fluvial activity occur for ~1/10 of target cross-section (space x time). Since 3.5 Gy, about 20 x D(181km) craters have occurred on Mars (Hartmann, 2005, Table 2). This predicts around 2 "Eberswaldes" on the whole planet. Given that this is a very rough estimate, our opinion is that the apparent uniqueness of Holden is consistent with this result.

8.4 Would *in situ* data from Eberswalde paleolake be still of interest?

Eberswalde crater was proposed for Mars Science Laboratory on the basis of a prolonged aqueous activity in the early Mars period. A few years ago, few paleolakes were as well documented as Eberswalde crater, and a landing site at the toe of the fan deposits was a logical choice early in the MSL site selection process (Grant et al., 2011). Nevertheless, our study raises doubts on the sustained activity of the paleolake as well as on its age, changing the scientific rationale for the site. The Martian geologic also record displays strong evidence for impact-induced fluvial activity – for example at Mojave crater (Williams and Malin, 2008) and at Sinton crater (Morgan & Head, 2009). It also shows strong evidence for sedimentary rock formation and perhaps fluvial activity extending over orbital timescales (e.g., Lewis *et al.*, 2008). It is not clear where Eberswalde falls. If we are to fully

924 exploit the paleoclimatic record encoded by Martian fluvial landforms, then the Eberswalde
925 example shows that better diagnostic tests will be needed in order to distinguish climatic from
926 impact triggering of fluvial activity.

927 The Late Hesperian Epoch during which Eberswalde paleolake was likely active may
928 have been dominated by episodic activities such as transient snowmelt post-dating the more
929 intense period of early Mars activity at the time of valley networks formation (e.g., Mangold et
930 al., 2004, 2008, Kite et al., 2011a,b, Howard and Moore, 2011, Mangold et al., 2012b).
931 Studying an example typical of this period is still of interest for the understanding of past
932 Mars, as well as for exobiology, in a well exposed stratigraphy. In the case that the Holden
933 impact led to regional warning, it would also be able to test hypotheses concerning such
934 process, as well as collect material from the older pre-Holden basin excavated by the impact.

935 However, exobiological interest may be limited by the lack of a sustained lake, the lack of
936 an obvious link with global fluvial activity, and the general cold climatic conditions expected
937 during this period. Since the first studies of Eberswalde crater (Malin and Edgett, 2003,
938 Moore et al., 2003), other locations have been studied that suggest more sustained aqueous
939 activity and so might be more rewarding for in-situ study. For example, much thicker
940 deposits (>500 m) are observed in depositional fans of Ismenius Cavus (Dehouck et al.,
941 2010) and in Terby crater (Ansan et al., 2011) with phyllosilicates being also present in these
942 paleolake deposits. Larger mineralogical diversity has been found in Columbus crater (Wray
943 et al., 2011) and in Jezero crater (Ehlmann et al., 2008). A higher phyllosilicate abundance
944 occurs at Mawrth Vallis (Poulet et al., 2008). The evidence discussed in this paper cannot
945 distinguish between short-lived climate versus impact triggers for the Eberswalde fan-delta.
946 In either case, Eberswalde crater should be considered as a location typical of relatively brief
947 late-stage episodes of aqueous activity at the surface of Mars but not as a location optimal
948 for sampling sustained aqueous activity.

949

9. Conclusions

The fan deposit in Eberswalde crater, north of Holden crater has been interpreted as strong evidence for sustained liquid water on Early Mars, during the Noachian period (Malin and Edgett, 2003). We have shown that the Holden impact is a key to understanding Eberswalde's fluvial and lacustrine activity. We find that:

(i) Stratigraphic relationships between Holden crater ejecta and Eberswalde's fluvial valleys and depositional fans support the conclusion that Holden formed before fluvial activity in Eberswalde.

(ii) Crater counts suggest that Holden crater formed probably near the beginning of the Late Hesperian, setting a maximum age for Eberswalde fluvial and lacustrine activity.

(iii) Drainage density in the catchment feeding the Eberswalde fan is far from uniform. Valley heads are especially concentrated close to Holden rim. Valleys are absent from the western part of the watershed as defined by HRSC topography. Possible explanations include: infiltration into the subsurface (possibly due to the presence of Holden ejecta); a short duration of fluvial activity at geological scale; or a spatially variable water input across the watershed.

(iv) Modeling of Eberswalde fan formation shows that a dilute flow should increase the water level and overflow the crater, contrary to observations of a nearly constant level of the paleolake. If flow was continuous, then a flow denser than expected for sinuous flows (S:W>0.01) is needed to match the data, and could also explain the putative transport of boulders within the fan.

(v) Any climatic explanation of the fluvial activity at Eberswalde should take into account formation in the Hesperian, which is thought to be a colder climate than was the Noachian. This implies that any lake would probably be quickly frozen, and favors hypotheses for valley formation involving episodic or regional processes (i.e.

977 volcanism, impact, unusual orbital forcing). Any hypothesis for fluvial activity at
978 Eberswalde should explain the apparent limited period of activity of the lake and
979 fan formation.

980 (vi) A possible scenario is that the Holden impact could have triggered fluvial activity by
981 local heating of pre-existing ground ice or surface ice. Ground ice and/or surface
982 ice are expected at Holden's latitude during past high obliquity periods.

983 (vii) The presence of highly erodible fractured bedrock (impact breccia of Holden)
984 need to be taken into account in modeling work because their low density and
985 mechanical weakness can explain a formation of valleys much faster here than in
986 locations with more intact bedrock possible transport of meter-sized blocks of
987 breccia, as well as a larger infiltration in the substratum.

988 (viii) Our study shows that the hydrated minerals found in Eberswalde sediments could
989 have originated by a variety of processes instead of being formed during short-
990 lived lacustrine activity. Indeed, these sediments were transported mainly from a
991 watershed eroding into Holden ejecta. Hydrated minerals could have been
992 excavated by the Holden impact from older pre-existing basins, or formed by
993 hydrothermal activity immediately after Holden formation.

994 Finally, while the Eberswalde paleolake cannot be used as an indicator for sustained
995 liquid water during the Noachian period, it is still of great interest for our understanding of
996 transient liquid water activity on Mars during subsequent periods.

997

998 **Acknowledgments**

999 *French authors thank the CNES and the INSU/CNRS through the PNP program and the*
1000 *Agence Nationale pour la Recherche through the grant* ANR-08-JCJC-0126 « *MadMacs". E.S.K.*
1001 *was supported by the O.K. Earl Fellowship at Caltech and by NASA grants NNX08AN13G*
1002 *and NNX09AN18G. M.G.K. gratefully acknowledges support from NWO-ALW / Netherlands*
1003 *Space Office. Modeling in section 5.4 done by M.G.K., modeling in section 7.3 done by*
1004 *E.S.K.. Authors thank John Grant and two anonymous reviewers for their insightful*
1005 *comments. We thank Melissa Rice for sharing a pre-publication Eberswalde manuscript.*
1006 *Initial results of this study were presented at the Fall 2010 (4th) and Spring 2011 (5th) Mars*
1007 *Science Laboratory (MSL) landing site selection workshops. Authors acknowledge the*
1008 *intellectual stimulation created by these workshops, and discussions generated by members*
1009 *of the fluvial "Tiger Team" of the MSL site selection, especially R. P. Irwin III for productive*
1010 *suggestions, without implying agreement with all ideas in this paper*

1011

Appendix A: summary of the fan model

The model has two independent components. The first is a calculation of flow discharge and sediment transport based on semi-empirical laws also used on Earth and summarized in Kleinhans (2005). The second component is a numerical code to store water and deposit sediment from a source into an impervious crater basin. When the water level in the basin rises, the subaqueous part of the deposit has a slope at the angle of repose, typically 0.3, whereas the subaerial part of the deposit maintains a fluvial slope, typically 0.01.

Appendix A1. Depositional fan and delta model

Kleinhans et al. (2010) present a quantitative morphological model for fan and delta formation that assumes as little as possible. The essential characteristic of a fan delta or alluvial fan is that sediment is fed into a basin where it is trapped because of the flow divergence. The horizontal flow divergence leads to a fan-shaped feature. Vertical flow divergence (depth) leads to deposition at the angle of repose. The shape of the alluvial fan and fan delta can therefore at first order be described as a relatively simple geometrical form. The shape of an alluvial fan can be approximated as an upright cone with a small top angle. The shape of the fan delta can be approximated as a truncated cone with a large top angle (namely, the subaqueous dynamic angle of repose) and the subaerial fluvial fan on top of this truncated cone can again be approximated as a cone with a small top angle similar to that of the alluvial fan. The plane where the subaerial cone is deposited on the subaqueous cone is

1037 at the water level. This plane is seen as the shoreline on the outside of the fan. The model
1038 calculates the growth of a sedimentary body in a crater lake, represented by a low-gradient,
1039 subaerial cone on top of a high-gradient, subaqueous cone without a top (called frustrum).

1040

1041 The setup of the model is as follows. Water and sediment are fed into a crater basin. The
1042 volumetric flux determines the volume of a fan or delta, which will be idealized with a 'fan on
1043 top of a truncated fan'. First, the water and sediment fluxes into the basin are calculated from
1044 semi-empirical relations applied to characteristics of the feeder channel. Second, a crater
1045 basin is defined based on empirical relations for crater depth and crater profile as a function
1046 of crater diameter. Overflow breaches as well as prefilling of craters by volcanic or impact or
1047 any other material are accounted for. Third, the crater basin is gradually filled with water at
1048 the estimated flux. Simultaneously, a conical fan is built up with sediment at the estimated
1049 flux (see A2). When the toe of the fan floods, a gentle-sloped subaerial cone is built on a
1050 steep truncated subaqueous cone with the intersection at the plane of the shoreline. Thus
1051 the rising water level of the lake determines the height of the shoreline and, as demonstrated
1052 in Kleinhans et al. (2010), the general shape of the deposit.

1053

1054 Small-scale morphology, such as crater wall irregularities, concavity of the fan surface and
1055 channel avulsion, is ignored. The model produces alluvial fans, stair-stepped fan deltas and
1056 Gilbert-type fan deltas depending on the presence of an overflowing breach in the crater rim.
1057 The parameters that determine which morphology emerges are the supply of sediment and
1058 water to the basin, the size of the basin and the duration of the flow. In principle the model
1059 can be fed with time-varying flow and sediment flux but for the present model runs it was
1060 kept entirely constant for lack of more information. The model was verified for a square basin
1061 by an analytical solution for a cone on top of a frustrum.

1062

The modeled crater basin is assumed be to point-symmetrical and to have a smooth wall with increasing gradient. The crater basin depth and profile (i.e. elevation between center point and crater rim) are calculated from empirical relations based on MOLA data (Garvin and Frawley, 1998). The shape of the crater basin is, however, unimportant, as long as it approximates the hypsometry (probability distribution of subaqueous bed surface elevation) of the real basin well enough to reproduce the water level rise for a given influx. Alluvial fans and fan deltas on Mars commonly occur in craters that have been breached, eroded and partially filled in. The above relations must therefore be modified in some cases for our model. Specifically, crater rims are often breached, so that the lake will not fill up to the rim as modeled with the above equations. This is incorporated as an overflow height (as a fraction of depth) above which the water will not rise. In addition, crater basins are often partially filled with sediment or rock of fluvial or volcanic origin. In our model this is incorporated as a prefilling height (as a fraction of depth). A plane horizontal crater floor is then assumed at this height. In the Figure 9, the overflow height (here about 230 m) was determined from the DEM as the lowest point in the crater rim and its effect can be seen in the dilute flow scenario results as the final water elevation at the delta shoreline (blue dots). The prefilling height in the crater (here about 80 m) can be seen in both scenarios as the flat horizontal crater floor (bold red line) on which the delta built up, above the smooth idealised crater floor. This prefilling height is also the lowest point observed in the DEM and the profile derived from HRSC data (green line). Both are accounted for in the numerical model.

A direct comparison between the cone model and HRSC DTM data for five deltas and an alluvial fan demonstrates that single-event dilute flows of short duration (days to years) have created all of the deposits described in Kleinhans et al. (2010). Two Gilbert fan deltas were formed in overspilling crater lakes from long low-gradient upstream channels. One alluvial fan was formed in a similar manner except that the damaged crater did not lead to ponding.

Three stair-stepped deltas were formed from short high-gradient upstream channels that only partially filled the crater lakes.

Appendix A2. Flow and sediment transport

The volume of the depositional model is constrained by the influx of sediment whilst the elevation of the break in slope, that is, the shoreline, is constrained by the influx of water. An impressive number of physics-based and semi-empirical relations for flow and sediment transport have been developed over the past two centuries, indicative of the limited understanding of turbulence and flow of water–sediment mixtures. The various equations and their limitations are described extensively in Kleinhans (2005) and one recommended combination is used to calculate flow conditions and sediment transport rate in a spreadsheet provided online with the Kleinhans et al. (2010) model paper.

The flow conditions can be calculated from the upstream channel characteristics width, depth and gradient. The hydraulic roughness is, in the absence of bars and subaqueous dunes, assumed to be related to the size of typical clasts found on Mars (Kleinhans, 2005). We use a median grain size of 0.1 m and a 90th percentile size of 0.6 m diameter. The main uncertainties are the hydraulic roughness and the flow depth, particularly where the flow may have been lower than bankfull. The uncertainty of flow discharge is estimated conservatively at a factor of 5 (Kleinhans, 2005). We assume that the crater basin is entirely water-tight and no significant evaporation takes place, so that all flow discharge is captured and retained.

Evaporation can safely be ignored (Kleinhans et al. 2010). From experiments and the well-known Ingersoll equation Sears and Moore (2005) found that evaporation in the present atmospheric conditions is 0.73 mm/h or 1.7×10^{-5} km/day. They calculate that an air temperature rise of 20°C increases the evaporation a factor of 2; a wind speed of 10 to 15 m/s increases evaporation a factor of 10; and evaporation decreases a factor of 10 for a ten-fold increase of air pressure. Even if an evaporation rate two orders of magnitude larger than calculated above is assumed, say, ~10^{-3} km/day or ~10^{-1} km/year, then the water loss from crater lakes by evaporation is still an order of magnitude smaller than the influx. Given that the flow discharge is only accurate within a factor of five, and that the delta shape resulting from a particular water–sediment ratio is not very sensitive, this effect can be ignored (Kleinhans et al., 2010).

A related issue to water loss by evaporation is a 'leaky cauldron' process: the crater floor may leak to some extent and the surrounding aquifer could accommodate the flow so that in extreme conditions the crater basin never has ponding water. However, the aquifer below crater floors may be expected to saturate quickly, after which the groundwater outflow is much slower than the fluvial inflow. Thus the leaky cauldron process is limited to the initial phase only where it may delay the onset of flooding the alluvial fan toe.

The sediment transport rate is calculated from the flow conditions and assumed sediment characteristics (Kleinhans, 2005). The transport rate is calculated as volumetric including pore space, which is assumed to be 0.2 for poorly sorted sediment. As there are very few particle size distributions available for Mars, we have to assume that distributions based on particle recognition and measurement in lander images are representative (see Kleinhans, 2005, for discussion). The main uncertainties stem from this unknown particle size distribution, the modeled flow conditions and the intrinsic uncertainty of sediment transport

predictors of at least a factor of 2. Hence the uncertainty of sediment flux is estimated conservatively at a factor of 10 (Kleinhans, 2005). The sediment transport predictors assume dilute flows, that is, low sediment concentrations that are entrained by an initially clear water flow. We used the classical Meyer-Peter & Mueller predictor for bedload transport, where the dominant mode of particle motion is sliding, rolling and saltating. An alternative option is to assume dense flows with high sediment concentrations of up to about 30% by volume. A dense flow implies that either an initially dilute flow exceeded the tremendous flow velocities necessary to cause massive suspension, or that sediment was supplied en masse to a flow from, e.g., a debris flow or other forms of mass wasting to the channel (Kleinhans 2005). A copy of the code used to generate these results is available from M.G.K.

Appendix B: Summary of the idealized model of post-impact runoff

Appendix B1. Generation of a lookup table for 1D column melt rate.

The initial condition for the idealized 1D Stefan model of melt production is instantaneous emplacement of a hot ejecta layer of thickness H and uniform temperature T_{ej} over a cold ice layer of infinite thickness.

We use a coordinate system that keeps the interface at (vertical coordinate) z=0. The interface moves downwards relative to the geoid as melting proceeds. Within each layer, Crank-Nicolson scheme is used to calculate advection and diffusion of material properties (temperature and density) relative to the interface. A Stefan boundary condition is imposed at the interface, giving the rate of melting (Q) of the ice. For a given model run, the

1163 sediment:water ratio of runoff (*S:W*) is fixed – the ice melt rate specifies the rate of
1164 entrainment of ejecta by the meltwater produced at the interface.

1165 The most significant assumptions and simplifications in this model are as follows. (i)
1166 The interface between the ejecta layer and the ice layer is smooth; (ii) meltwater production
1167 is steady and there is no attempt to model explosive molten fuel-coolant interactions; (iii) no
1168 water vapor is produced; (iv) sediment and water runoff is assumed to be removed from the
1169 column as soon as it is produced at the interface – it does not pond at the interface nor does
1170 it flow through the ejecta layer; (v) T_{ej} is uniform with depth within the ejecta blanket.

1171 Ejecta (the top layer) has density ρ_{ej} = 2500 kg/m^3, specific heat capacity $C_{p,ej}$ = 840
1172 J/°C/kg, and thermal conductivity 1.7 W/m/°C. Ice (the bottom layer) has ρ_i = 910 kg/m^3, $C_{p,i}$
1173 = 1751 J/°C/kg, thermal conductivity 2.5 W/m/°C, and latent heat L = 3.34 x 10^5 J/kg. The
1174 interface between ejecta and rock is assumed to be buffered at the melting point T_m = 0 °C.
1175 We carried out a parameter sweep with H ranging from 25-400 m, *S:W* ranging from 0.005-1,
1176 and T_{ej} ranging from 0°C to 1000°C. Values of T_{ej} close to 0°C do not produce meltwater
1177 because heat is conducted into the ice away from the interface.

1178 The parameter sweep shows that the model has two endmember behaviors. For
1179 small *S:W*, the model output approximates half-space cooling of the ejecta by the melting ice,
1180 accelerated by conductive loss of heat through the top of the ejecta. In this limit, discharge Q

1181 $\propto t^{0.5}$. As sediment:water ratio increases, removal of ejecta by melted ice becomes

1182 important. Positive feedback between erosional mining of heat from the 'warm core' of the
1183 ejecta blanket, and increased thermal erosion, leads to an increase in the melt rate (Kite et
1184 al. 2011a) and a shallowing of the fall-off of Q with t. Provided that the Stefan number
1185 exceeds one ($St = T_{ej}\ C_{p,ej} / (L + C_{p,i} (T_m - T_i))$), giving $St > 1$ for $T_{ej} > 530$°C), a thermal

1186 runaway occurs in the debris flow limit ($S:W \rightarrow$ ~1), with very rapid erosion of the majority of
1187 the ejecta blanket by meltwater.

1188

1189 **Appendix B2. Summing 1D model over the Eberswalde catchment.**

1190

1191 To sum the 1D column output over the Eberswalde catchment, we need to know H and T_{ej} at
1192 each point in the watershed. We use the semi-analytic Rayleigh-Z ejecta model to find H as a
1193 function of distance from Holden. This assumes an axisymmetric distribution of ejecta. Our
1194 approach closely follows Barnhart et al. (2010) and Barnhart & Nimmo, (2011). Crater radius
1195 was set to 77.5km, and impact velocity to 7 km/s. Predicted H with this Rayleigh-Z method is
1196 comparable to the McGetchin et al. (1973) lunar scaling. The Barnhart et al. (2010) and
1197 Barnhart & Nimmo, (2011) equations and parameters can also be used to find T_{ej}, assuming
1198 that the shock-heated rock temperature is also the temperature of the ejecta. For a crater of
1199 Holden's size, the predicted ejecta temperatures are very high, and are sensitive to the
1200 exponent of peak-pressure falloff (Barnhart et al., 2010). It is necessary to reduce T_{ej} to ≤
1201 600°C to produce a reasonable match to observations. This might correspond to either (1)
1202 unrealistically high temperature predictions from the Rayleigh-Z parameterization, or (2) loss
1203 of ejecta thermal energy to atmospheric heating, atmospheric shocks, and water vapor
1204 production.

1205 We use the Rayleigh-Z H and a fixed T_{ej} to interpolate within the look-up table for the
1206 appropriate $Q(t)$ and sum the results. The sum is then weighted by the area of the
1207 Eberswalde main fan catchment within annuli concentric on the center of Holden Crater. To
1208 find these areas, we used a catchment corresponding to the convex hull of the largest
1209 channels draining into the Eberswalde main fan. (The HRSC and MOLA topographically-
1210 defined watersheds are more extensive than the convex hull of the largest channels, and so
1211 produce more runoff when used to drive the model. However, given the lack of visible

channels in the added region, it is not clear whether they did in fact contribute runoff to Eberswalde's fan).

A copy of the code used to generate these results is available for unrestricted further use from E.S.K.

References

Abramov, O., Kring D. A., 2005. Impact-induced hydrothermal activity on early Mars, JGR, 110, E12S09.

Alexiades, V., 1992. Mathematical Modeling Of Melting And Freezing Processes, CRC Press.

Ansan, V., Mangold, N., 2006. New observations of Warrego Valles, Mars: Evidence for precipitation and surface runoff, Planet. Space Science, 54, 219-242.

Ansan, V., Mangold, N., Masson, Ph., Gailhardis, E., and Neukum, G., 2008. Topography of valley networks on Mars from the Mars Express High Resolution Stereo Camera digital elevation models, J. Geophys. Res.-Planets, 113, E07006.

Ansan, V., Loizeau, D., Mangold, N., Le Mouélic, S., Carter, J., Poulet, F., Dromart, G., Lucas, A., Bibring, J.-P., Gendrin, A., Gondet, B., Langevin, Y., Masson, Ph., Murchie, S., Mustard, J.F., Neukum, G., 2011. Stratigraphy, mineralogy, and origin of layered deposits inside Terby crater, Mars. Icarus, 211, 273-304.

Baker, V.R., and Partridge, J.B., 1986. Small Martian Valleys - Pristine And Degraded Morphology, J. Geophys. Res. 91 (B3) 3561-3572.

Baker, V. R., Strom, R. G., Gulick, V. C., Kargel, J. S., Komatsu, G., Kale, V. S. 1991. Ancient oceans, ice sheets and the hydrological cycle on Mars, Nature, 352, 589– 594.

Balme, M., Mangold, N., Baratoux, D., Costard, F., Gosselin, M., Masson, Ph., Pinet, P., Neukum, G., 2006. Orientation and Distribution of Recent Gullies in the Southern Hemisphere

of Mars: Observations from HRSC/MEX and MOC/MGS Data, J. Geophys. Res-Planets, 111, E5, E05001.

Baratoux, D., N. Mangold, P. Pinet, F. Costard, 2005. Thermal Properties of Lobate Ejecta in Syrtis Major, Mars: Implications for the Mechanisms of Formation J. Geophys. Res., 110 (E4), E04011.

Baratoux, D., C. Delacourt, and P. Allemand, 2002. An instability mechanism in the formation of the Martian lobate craters and the implications for the rheology of ejecta, Geophys. Res. Lett., 29(8), 1210, doi:10.1029/2001GL013779.

Barlow, N. G., 1994. Sinuosity of Martian rampart ejecta deposits, J. Geophys. Res., 99(E5), 10,927– 10,935.

Barlow, N. G., and T. L. Bradley, 1990. Martian impact craters: Correlations of ejecta and interior morphologies with diameter, latitude and terrain, Icarus, 87, 156– 179.

Barnhart, C. J., Nimmo, F., & Travis, B. J. (2010). Martian post-impact hydrothermal systems incorporating freezing. Icarus 208, 101-117,doi:10.1016/j.icarus.1010.01.013.

Barnhart, C. J., Nimmo, F. (2011). Role of impact excavation in distributing clays over Noachian surfaces. J. Geophys. Res. 116, E01009, doi:10.1029/2010JE003629.

Bhattacharya et al., 2005 J.P. Bhattacharya, T.H.D. Payenberg, S.C. Lang and M. Bourke, Dynamic river channels suggest a long-lived Noachian crater lake on Mars, *Geophysical Research Letters* **32** (2005), pp. 1–4

Bibring, J.P., Langevin, Y., Mustard, J. F., Poulet, F., Arvidson, R., Gendrin, A., Gondet, B., Mangold, N., Pinet, P., Forget, F., and the OMEGA team, 2006. Global Mineralogical and Aqueous Mars History derived from the OMEGA/Mars Express data. Science, 312, 400-404.

Bouley, S., Ansan, V., Mangold, N., Masson, Ph., Neukum G., 2009. Fluvial morphology of Naktong Vallis, Mars: A late activity with multiple processes, Planet. Space Science, 57, 982-999.

1262 Bouley, S., Craddock, R. C., Mangold, N., Ansan, A., 2010. Characterization Of Fluvial Activity
1263 In Parana Valles Using Different Age-Dating Techniques, Icarus, 207 (2) 686-698.

1264 Brakenridge, G. R., Newsom, H. E., Baker, V. C., 1985. Ancient hot springs on Mars: Origins
1265 and paleoenvironmental significance of small Martian valleys, Geology, 13, 859-861.

1266 Buhler, P. B., Fassett, C.I., Head, J.W., & Lamb, M.P 2011. Evidence for paleolakes in
1267 Erythraea Fossa, Mars: Implications for an ancient hydrological cycle. Icarus 213, 104-115

1268 Byrne, S. *et al.*, 2009. Distribution of Mid-Latitude Ground Ice on Mars from New Impact
1269 Craters, Science, 325, 1674-1676.

1270 Cabrol, N., Grin, E., 1999. Distribution, classification and ages of Martian impact crater lakes.
1271 Icarus 142, 160–172.

1272 Carr, M. H. , 1996. Water on Mars, 229 pp., Oxford Univ. Press, New York.

1273 Carr, M.H., Crumpler, L.S., Cutts, J.A., Greeley, R., Guest, J.E., Masursky, H., 1977. Martian
1274 impact craters and emplacement of ejecta by surface flow. J. Geophys. Res., 82, 4055-4065.

1275 Colella A., Prior D.B., 1990. Coarse-grained deltas, Spec Publ IAS 10, Blackwell, Oxford.

1276 Cook, C. M., H. J. Melosh, W. F. Bottke Jr.,2003. Doublet craters on Venus Icarus 165, 90–
1277 100.

1278 Costard, F. M., 1989. The Spatial Distribution of Volatiles in The Martian Hydrolithosphere,
1279 Earth Moon Planets, 45, 265.

1280 Costard, F., F. Forget, N. Mangold, J.-P. Peulvast, Formation of recent Martian debris flows by
1281 melting of near-surface ground ice at high obliquity, Science, 295, 110–113, 2002.

1282 Craddock, R.A., Maxwell, T.A., and Howard, A.D., 1997. Crater morphometry and modification
1283 in the Sinus Sabaeus and Margaritifer Sinus regions of Mars, J. Geophys. Res., 102, E2,
1284 4161-4183.

1285 Craddock, R. A. Howard, A. D., 2002. The case for rainfall on a warm, wet early Mars, J.
1286 Geophys. Res. 107 JE001505.

1287 Dehouck, E., Mangold, N., Le Mouélic, S., Ansan, V., Poulet, F., 2010. Ismenius Cavus, Mars:
1288 A deep paleolake with phyllosilicate deposits, Planet. Space Sci., 58 (6) 941-946.

1289 Doran, P.T., Berry Lyons, W., & McKnight, D.M. (Eds.), 2010. Life in Antarctic Deserts and
1290 other Cold Dry Environments: Astrobiological Analogs, Cambridge Astrobiology (No. 5),
1291 Cambridge University Press.

1292 Duxbury, T.C., Kirk, R.K., Archinal, B.A., Neumann, G.A., 2002. Mars geodesy/ cartography
1293 working group recommendation on Mars cartographic constants and coordinate systems. In:
1294 Symposium on Geospatial Theory. Processing andApplication. Ottawa, p. 4.

1295 Ehlmann, B.L., Mustard, J.F., Fassett, C.I., Schon, S.C., Head, J.W., Desmarais, D.J., Grant,
1296 J.A., Murchie, S.L., 2008. Clay minerals in delta deposits and organic preservation potential on
1297 Mars. Nat. Geosci. 1, 355–358.

1298 Engelhardt, W. V. ; Arndt, J., Fecker, B., Panckau, H. G., 1994. Ries impact crater, Germany:
1299 Thermal history of the suevite breccia , Meteoritics, 29, 463.

1300 Fassett, C. I., and Head, J., W., 2008. The timing of martian valley network activity:
1301 Constraints from buffered crater counting. Icarus, 195, 61-89.

1302 Fassett, C. I., Dickson J.A., Head, J.W., Levy, J.S., Marchant, D.R., 2010. Supraglacial and
1303 proglacial valleys on Amazonian Mars, Icarus, 208, 86-100.

1304 Freeth, S. J., and K. O. Ladipo, The development and restoration of syn-sedimentary faults,
1305 Earth Planet. Sci. Let., 78, 411-419.

1306 Garvin, J. B., and J. F. Frawley (1998), Geometric properties of Martian impact craters:
1307 Preliminary results from the Mars Orbiter Laser Altimeter, Geophys. Res. Lett., 25, 4405,
1308 doi:10.1029/1998GL900177.

1309 Grant, J.A., 1987, The geomorphic evolution of Eastern Margaritifer Sinus, Mars: in Advances
1310 in planetary geology: NASA Technical Memorandum 89871, pp. 1-268.

1311 Golombek, M.P., et al., 2006. Erosion rates at the Mars Exploration Rover landing sites and
1312 long-term climate change on Mars. J. Geophys. Res., 111, E12S10.

1313 Grant, J.A., and Parker, T.J., 2002, Drainage Evolution of the Margaritifer Sinus Region, Mars,
1314 J. Geophys. Res., 107, 10.1029/2001JE001678.

1315 Grant, J. A., et al., 2008. HiRISE imaging of impact megabreccia and sub-meter aqueous
1316 strata in Holden Crater, Mars, Geology, 36, 195.

1317 Grant, J.A., Golombek, M. P., Grotzinger, J. P., Wilson, S. A., Watkins, M. M., Vasavada, A.
1318 R., Griffes, J. L., Parker, T. J., 2011. The science process for selecting the landing site for the
1319 2011 Mars Science Laboratory. Planetary and Space Science**,** 59, (11-12)1114-1127.

1320 Grant, J. A., and Wilson S. A., 2011. Late alluvial fan formation in southern Margaritifer Terra,
1321 Mars, Geophys. Res. Letters, 38, L08201, DOI: 10.1029.

1322 Gulick, V. C., Baker, V. R., 1990. Origin and evolution of valleys on Martian volcanoes, J.
1323 Geophys. Res. 95, 14325.

1324 Gwinner, K., Scholten, F., Jaumann, R., Roatsch, T., Oberst, J., Neukum, G., 2007. Global
1325 mapping of Mars by systematic derivation of Mars Express HRSC High-Resolution Digital
1326 Elevation Models and orthoimages. ISPRS Commission IV, Working Group 9, Extraterrestrial
1327 Mapping Workshop ‘‘Advances in PlanetaryMapping”, Houston, Texas.

1328 Hall, Brenda L.; Denton, George H.; Fountain, Andrew G.; et al., 2010. Antarctic lakes suggest
1329 millennial reorganizations of Southern Hemisphere atmospheric and oceanic circulation.
1330 Proceedings of the National Academy of Sciences, 107, 21355-21359,
1331 10.1073/pnas.1007250107.

1332 Hartmann, W.K., Neukum, G., 2001. Cratering chronology and the evolution of Mars. Space
1333 Sci. Rev. 96, 165–194.

1334 Hauber, E., Reiss, D., Ulrich, M., Preusker, F., Trauthan, F., Zanetti, M., Hiesinger, H.,
1335 Jaumann, R., Johansson, L., Johnsson, A., Gasselt, S., Olvmo, M., 2011. Landscape
1336 evolution in Martian mid-latitude regions: insights from analogous periglacial landforms in
1337 Svalbard. In: Balme, M.R., Bargery, A.S., Gallagher, C.J., Gupta, S. (Eds.), Martian
1338 Geomorphology. Geological Society, London, Special Publications, 356, pp. 111–131.
1339 doi:10.1144/SP356.7.

1340 Howard, A. D., Moore, J. M., 2011. Late Hesperian to early Amazonian midlatitude Martian
1341 valleys: Evidence from Newton and Gorgonum basins J. Geophys. Res. Planets, 116,
1342 E05003, DOI: 10.1029/2010JE003782.

1343 Howard, A.D., Moore, J. M., Irwin, R. P., Dietrich, W. E., 2007. *Lunar Planet. Sci. Conf.* 38,
1344 Abstract 1168.

1345 Hoyal, D. C. J. D., and B. A. Sheets (2009), Morphodynamic evolution of experimental
1346 cohesive deltas, J. Geophys. Res.,114, F02009, doi:10.1029/2007JF000882.

1347 Hynek, B.M., Phillips, R.J., 2001. Evidence for extensive denudation of the martian highlands.
1348 Geology, 29, 407–410.
1349 Irwin, R. P., Craddock R.A., Howard, A.D., 2005. Interior channels in Martian valley networks:
1350 Discharge and runoff production, Geology, 33 (6) 489–492.

1351 Ivanov, B. A., 2001. Mars/Moon Cratering Rate Ratio Estimates, Space Science Reviews, 96,
1352 87–104.

1353 Jerolmack, D. J., Mohrig, D., Zuber, M. T., Byrne, S., 2004. A minimum time for the formation
1354 of Holden Northeast fan, Mars, Geophysical. Res. Letters, 31 (21) L21701.

1355 Jones, A. P., McEwen, A.S., Tornabene, L.L., Baker, V.R., Melosh, H. J., Berman, D.C., 2011.
1356 A geomorphic analysis of Hale crater, Mars: The effects of impact into ice-rich crust, Icarus,
1357 211, 259-272.

1358 Kadish, S.J., Head, J.W., & Barlow, N.G., 2010. Pedestal crater heights on Mars: A proxy for
1359 the thicknesses of past, ice-rich, Amazonian deposits, Icarus 210, 92-101.

1360 Kim, W., and Jerolmack, D.J., 2008. The pulse of calm fan deltas. Journal of Geology 116,
1361 315-330.

1362 Kite, E.S., Michaels, T.I., Rafkin, S.C.R., Manga, M., and Dietrich, W.E. 2011a. Localized
1363 precipitation and runoff on Mars. Journal of Geophysical Research, 116, E07002.
1364 doi:10.1029/2010JE003783.

1365 Kite, E.S., Rafkin, S.C.R., Michaels, T.I., Dietrich, W.E., and Manga, M. 2011b. Valles
1366 Marineris chaos, storms, and past climate on Mars. Journal of Geophysical Research, in
1367 press. doi:10.1029/2010JE003792

1368 Kleinhans, M.G., van Rijn, L.C., 2002. Stochastic prediction of sediment transport in sand-
1369 gravel bed rivers, J. Hydraul. Eng., 128 (4), 412-425, doi:10.1061/(ASCE)0733-9429,
1370 128:4(412) .

1371 Kleinhans, M. G., 2005. Flow discharge and sediment transport models for estimating a
1372 minimum timescale of hydrological activity and channel and delta formation on Mars, J.
1373 Geophys. Res., Planets, 110 E2, E12003.

1374 Kleinhans, M.G., H.E. van de Kasteele and E. Hauber, 2010. Palaeoflow reconstruction from
1375 fan delta morphology on Mars, Earth and Planetary Science Letters 294, 378-392,
1376 doi:10.1016/j.epsl.2009.11.025.

1377 Koeberl, C., H. Henkel (eds.) (2005) Impact faulting. Springer, Berlin-Heidelberg.

1378 Kraal, E. R., Bredt, A., Moore, J. M., Howard, A. H., and Asphaug, E. A. 2008a, Catalogue of
1379 large alluvial fans in Martian impact craters. Icarus, 194, Issue 1,
1380 doi:10.1016/j.icarus.2007.09.028

1381 Kraal, E.R., van Dijk, M., Postma, G., Kleinhans, M.G., 2008b. Martian stepped-delta
1382 formation by rapid water release. Nature 451, 973-976

1383 Kraal, E.R., and Postma, 2008. The challenge of explaining Meander bends in the Eberswalde
1384 delta, *Lunar Planet. Sci. Conf.,* **39**, Houston, 1897.

1385 Kuhnle, R. A., 1993. Incipient motion of sand-gravel sediment mixtures. J. Hydraul. Eng., 119
1386 (12) 1400-1415.

1387 Laskar, J., Correia, A.C.M., Gastineau, M., Joutel, F. Levrard, B., Robutel, P., 2004. Long term
1388 evolution and chaotic diffusion of the insolation quantities of Mars, Icarus, 170, 343-364,
1389 doi=10.1016/j.icarus.2004.04.005

1390 Lewis K.W. Aharonson O., 2006. Stratigraphic analysis of the distributary fan in Eberswalde
1391 crater using stereo imagery, J. Geophys. Res., Planets, 111 (E6) E06001.

1392 Lewis, K. W., O. Aharonson, J. P. Grotzinger, R. L. Kirk, A. S. McEwen, T.-A. Suer (2008), Quasi-
1393 Periodic Bedding in the Sedimentary Rock Record of Mars *Science, 322* (5907), 1532-1535

1394 Loesch, T. N. (2001), Hydrologic Analysis Using GIS. Minnesota GIS/LIS Consortium, Spring
1395 Workshop, Alexandria, Minnesota, USA.

1396 Loizeau, D., Mangold, N., Poulet, F., Ansan, V., Hauber, E., Bibring, J.-P., Gondet, B.,
1397 Langevin, Y., Masson, Ph., Neukum, G., 2010. Stratigraphy in the Mawrth Vallis region
1398 through OMEGA, HRSC color imagery and DTM, Icarus, 205 (2), 396-418.

1399 Loizeau D., Mangold, N., Poulet, F., Bibring, J.-P., Gendrin, A., Ansan, V., Gomez, C.,
1400 Langevin, Y., Gondet, B., Masson, Ph, Neukum, G., 2007. Phyllosilicates in the Mawrth Vallis
1401 region of Mars, J. Geophys. Res., 112, E.08S08.

1402 Lorenz, R. D., Kraal, E. R., Eddlemon, E. E., Cheney, J., and Greeley, R., 2005, Sea-surface
1403 wave growth under extraterrestrial atmospheres - Preliminary wind tunnel experiments with
1404 applications to Mars and Titan: Icarus. 175, 556.

1405 Macke, R. J., Kiefer, W. S., Britt, D. T., Irving, A. J., Consolmagno, G. J., 2011. Densities,
1406 Porosities And Magnetic Susceptibilities Of Meteoritic Lunar Samples: Early Results. Lunar
1407 Planet. Sci. Conf, Houston, 43, abstract N°1986.

1408 Mahoney, A., Eicken, H., Shapiro, L., and Grenfell, T. C., 2004. Ice motion and driving forces
1409 during a spring ice shove on the Alaskan Chukchi coast. Journal of Glaciology, Vol 50, No
1410 169. P 195 – 207.

1411 Malin, M.C. et al., 1998. Early views of the martian surface from the Mars Orbiter Camera of
1412 Mars Global Surveyor. Science 279, 1681–1685.

1413 Malin, M. C., Edgett, K. S., 2003. Evidence for persistent flow and aqueous sedimentation on
1414 early Mars, Science, 302, 1931, 2003.

1415 Malin, M. C. *et al.*, 2007. Context Camera Investigation on board the Mars Reconnaissance
1416 Orbiter, *J. Geophys. Res.*, 112, E05S04.

1417 Mangold, N., 2003. Geomorphic analysis of lobate debris aprons on Mars at MOC scale:
1418 evidence for ice sublimation initiated by fractures. *J. Geophys. Res. Planets* **108** (E4), 2-1.

1419 Mangold N., P. Allemand, P. Thomas, P. Duval et Y. Géraud, 2002. Experimental and
1420 theoretical deformation of ice-rock mixtures: implications on rheology and ice content of
1421 Martian permafrost, *Planetary and Space Science,* 50, 385-401, 2002.

1422 Mangold, N., Quantin, C., Ansan, V., Delacourt, C., Allemand, P., 2004. Evidence for
1423 precipitation on Mars from dendritic valleys in the Valles Marineris area, Science, 305, 78-81.

1424 Mangold, N., Ansan, V., Masson, Ph., Quantin, C., and Neukum, G., 2008. Geomorphic study
1425 of fluvial landforms on the northern Valles Marineris plateau, Mars, J. Geophys. Res.,
1426 doi:10.1029/2007JE002985, 113, E08009.

1427 Mangold, N., F. Poulet, J. Mustard, J-P. Bibring, B. Gondet, Y. Langevin, V. Ansan, Ph.
1428 Masson, C. Fassett, J. Head, H. Hoffmann, G. Neukum, 2007. Mineralogy of the Nili Fossae
1429 region with OMEGA/MEx data: 2. Aqueous alteration of the crust, *J. Geophys. Res.*, 112,
1430 E08S04.

1431 Mangold, N., Ansan, V., 2006. Detailed study of an hydrological system of valleys, a delta and
1432 lakes in Thaumasia region, Mars, Icarus, 180, 75-87.

1433 Mangold, N. 2012. Fluvial landforms on fresh impact crater ejecta. Planetary Space Science,
1434 62 (1) 69-85.

1435 Mangold, N.; Carter, J.; Poulet, F.; Ansan, V.; Loizeau, D, 2012a. Late Hesperian aqueous
1436 alteration at Majuro crater, Mars, Planet.Space. Sci., in press.

1437 N. Mangold, S. Adeli, S. Conway, V. Ansan, and B. Langlais, 2012, A chronology of early Mars
1438 climatic evolution from impact crater degradation, J. Geophys. Res., 117, E4,
1439 doi:10.1029/2011JE004005, 2012b.

1440 Marzo, G. A., Davila A. F.,Tornabene L. L., Dohm, J. M., Fairen, A. G., Gross, C., Kneissl, T.,
1441 Bishop, J. L., Roush, T.L., McKay, C.P., 2010. Evidence for Hesperian impact-induced
1442 hydrothermalism on Mars, Icarus, 208 (2) 667-683.

1443 Matsubara, Y., Howard, A. D., Drummond, S. A., 2011. Hydrology of early Mars: Lake basins
1444 J. Geophys. Res. Planets, 116, E04001, DOI: 10.1029/2010JE003739.

1445 McEwen, A.S. et al., 2007. Mars Reconnaissance Orbiter's High Resolution Imaging Science
1446 Experiment (HiRISE). J. Geophys. Res. 112, E05S02. doi:10.1029/2005JE002605.

1447 McEwen, A., Grant, J., Mustard, J., Wray, J., Tornabene, L., 2009. Early Noachian rocks in
1448 megabreccia deposits on Mars, European Planetary Science Congress Abstracts, Vol. 4,
1449 EPSC2009-50 4-2, 2009.

1450 McGetchin T.R., Settle, M., Head, J.W., 1973. Radial thickness variation in impact crater
1451 ejecta: implications for lunar basin deposits, Earth. Planet. Sci. Letters, 20 (2) 226-236.

1452 Melosh, H. J., 1989. Impact cratering: A geologic process, Oxford Univ. Press, 244p.

1453 Meresse, S., F. Costard, N. Mangold, D. Baratoux, J. M. Boyce, (2006) Martian perched craters
1454 and large ejecta volume: evidence of episodes of deflation of the northern lowlands,
1455 *Meteoritics and Planetary science* 41.

1456 Michael and Neukum, 2010. Planetary surface dating from crater size–frequency distribution
1457 measurements: Partial resurfacing events and statistical age uncertainty. Earth and Planetary
1458 Science Letters 294, 223–229.

1459 Milliken, R., and D. Bish, 2010. Sources and sinks of clay minerals on Mars, Philos. Mag., 90,
1460 2293, doi:10.1080/14786430903575132.

1461 Moore, J. M., and Wilhelms, D. E., 2001. Hellas as a possible site of ancient ice-covered
1462 lakes on Mars. Icarus 154, 258-276.

1463 Moore, J.M., Howard, A.D., Dietrich, W.E., Schenk, P. M. 2003. Martian layered fluvial
1464 deposits: Implications for Noachian climate scenarios, 30 (24) 2292.

1465 Moore, J. M., Howard, A. D. 2005. Large alluvial fans on Mars, J. Geophys. Res., 110,
1466 E04005, doi:10.1029/2005JE002352.

1467 Morgan G. A., Head, J. W., 2009. Sinton crater, Mars: Evidence for impact into a plateau
1468 icefield and melting to produce valley networks at the Hesperian-Amazonian boundary, Icarus,
1469 202, 39.

1470 Mouginis-Mark, P. J., 1987. Water or Ice in The Martian Regolith - Clues From Rampart
1471 Craters Seen At Very High-Resolution, Icarus, 71, 268-286.

1472 Murray C. D., and S. F. Dermott, 2000, Solar System Dynamics, Cambridge Univ. Press, ISBN 0-
1473 521-57597-49780521575973.

1474 Mustard, J. F. *et al.*, 2001. Evidence for recent climate change on Mars from the identification
1475 of youthful near-surface ground ice, Nature, 412, 411-413.

1476 Mustard, J. F., Ehlmann, B. L., Murchie, S. L., Poulet, F., Mangold, N., Head, J. W., Bibring,
1477 J.-P., Roach, L. H., 2009. Composition, Morphology, and Stratigraphy of Noachian Crust
1478 around the Isidis basin, J. Geophys. Res., doi:10.1029/2009JE003349.

1479 Muttik N., Kirsimäe K., Torsten W., Vennemann, 2010, Stable isotope composition of smectite
1480 in suevites at the Ries crater, Germany: Implications for hydrous alteration of impactites, Earth
1481 Planet. Sci. Letters,

1482 Neukum, G., Jaumann, R., and HRSC Co-Investigator Team, 2004. HRSC: The High
1483 Resolution Stereo Camera of Mars Express. In: Wilson, A. (Ed.), Mars Express: The Scientific
1484 Payload. ESA SP-1240, Noordwijk, Netherlands: ESA Publications Division, pp. 17–36. ISBN
1485 92-9092-556-6.

1486 Neukum, G., *et al.*, 2004. Recent and episodic volcanic and glacial activity on Mars revealed
1487 by the High Resolution Stereo Camera, Nature, 432, 971-975.

1488 Newsom, H. E., 1980. Hydrothermal Alteration of Impact Melt Sheets With Implications For
1489 Mars, Icarus, 44 (1) 207-216.

1490 Newsom, H.E., Britelle, G.E., Hibbitts, C.A., Crossey, L.J. and Kudo, A.M., 1996.
1491 Impact cratering and the formation of crater lakes on Mars. J. Geophys. Res.-Planets,
1492 101, 14,951-14,955.

1493 Newsom, H.E., 2010. Heated lakes on Mars, in Lakes on Mars, edited by Nathalie
1494 Cabrol and Edmond Grin, Elsevier, Amsterdam, pp. 91-110, ISBN 978-0-444-52854-4

1495 Pierson, T.C. (Editor) (1997). Hydrologic consequences of hot rock-snowpack interactions at
1496 Mount St. Helens Volcano, Washington, 1982-84, U.S. Geological Survey Open-File Report
1497 96-179.

1498 Plaut, J.J., Picardi, G., Safaeinili, A., Ivanov, A.B., Milkovich, S.M., Cicchetti, A., Kofman, W.,
1499 Mouginot, J. Farrell, W.M. and Phillips, R.J. Clifford, S.M., Frigeri, A., Orosei, R., Federico, C.,
1500 Williams, I.P., Gurnett, D.A., Nielsen, E., Hagfors, T. and Heggy, E. Stofan, E.R., Plettemeier,
1501 D., Watters, T.R. and Leuschen, C.J., Edenhofer, P., 2007, Subsurface Radar Sounding of the
1502 South Polar Layered Deposits of Mars, Science,316, 92, doi=10.1126/science.1139672.

1503 Pondrelli, M., Rossi, A.P., Marinangeli, L., Hauber, E., Gwinner, K., Baliva, A., Di Lorenzo, S.,
1504 2008. Evolution and depositional environments of the Eberswalde fan delta, Mars, Icarus, 197
1505 (2) 429-451.

1506 Pondrelli M., Rossi, A.P., Platz, T., Ivanov, A., Marinangeli, L., Baliva A., 2011**.** Geological,
1507 geomorphological, facies and allostratigraphic maps or the Eberwalde fan delta, Planet. Spa.
1508 Sci., 59 (11-12) 1166-1178.

1509 Poulet, F., Bibring, J.-P., Mustard, J. F., Gendrin, A., Mangold, N., Langevin, Y., Arvidson, R.
1510 E., Gondet, B., Gomez, C., and the OMEGA Team, 2005. Phyllosilicates on Mars and
1511 Implications for the Early Mars History, Nature, 438, 623-628, 2005.

1512 Poulet, F., N. Mangold, D. Loizeau, J.-P. Bibring, Y. Langevin, J. Michalski, and B. Gondet,
1513 Abundance of minerals in the phyllosilicate-rich units on Mars, *Astronomy & Astrophysics*,
1514 487, L41–L44, 2008.

1515 Pravec, P., and 55 co-authors, 2006, Photometric survey of binary near-Earth asteroids,
1516 Icarus, 181, (1) 63-93, DOI: 10.1016/j.icarus.2005.10.014.

1517 Pravec, P., and 39 co-authors, 2012. Binary Asteroid Population. 2. Anisotropic distribution of
1518 orbit poles. Icarus 218, 125–143.

1519 Quantin, C., Allemand, P., Mangold, N., Dromart, G. Delacourt, C., 2005. Fluvial and
1520 lacustrine activity on layered deposits in Melas Chasma, Valles Marineris, Mars, J. Geophys.
1521 Res., 110, E12S19.

1522 Reimnitz, E., P.W. Barnes and J. R. Harper. 1990. A review of beach nour- ishment from ice
1523 transport of shoreface materials, Beaufort Sea, Alaska. J. Coast. Res., 6(2), 439 -470.

1524 Rice, M. S., S. Gupta, J. F. Bell III, and N. H. Warner (2011), Influence of fault-controlled
1525 topography on fluvio-deltaic sedimentary systems in Eberswalde crater, Mars, *Geophys. Res.*
1526 *Lett.*, 38, L16203, doi:10.1029/2011GL048149.

1527 Saunders S. R. (1979) USGS Misc. Inv. Series I–1144, 1:5,000,000.

1528 Schultz, P. H., R. A. Schultz, and J. L. Rogers (1982), Structure and evolution of ancient impact
1529 basins on Mars, *J. Geophys. Res.*, *87*, 9803-9820.

1530 Scholten, F., Gwinner, K., Roasch, T., Matz, K.-D., Wählisch, M., Giese, B., Oberst, J.,
1531 Jaumann, R., Neukum, G., and HRSC Co-Investigator Team, 2005. Mars ExpressHRSC data
1532 processing. Photogram. Eng. Rem. Sens. 71 (10), 1143–1152.

1533 Segura, T. L., Toon, O. B., Colaprete, A., Zahnle, K., 2002. Environmental effects of large
1534 impacts on Mars, Science, 298, 1977-1980.

1535 Sears, D. W. G., and S. R. Moore (2005), On laboratory simulation and the evaporation rate of
1536 water on Mars, Geophys. Res. Lett., 32, L16202,doi:10.1029/2005GL023443.

1537 Segura, T.L., Toon O.B., Colaprete, A., 2008. Modeling the environmental effects of moderate-
1538 sized impacts on Mars. J. Geophys. Res. 113:E11007.

1539 Selvans, M.M., Plaut, J.J. Aharonson, O.,Safaeinili, A., 2010. Internal structure of Planum
1540 Boreum, from Mars advanced radar for subsurface and ionospheric sounding data, Journal of
1541 Geophysical Research- Planets, 115, E14,E09003, 9003, doi=10.1029/2009JE003537.

1542
1543 Smith, D. E., et al., 1999. The global topography of Mars and implications for surface
1544 evolution, Science, 284, 1495 – 1503.

1545 Squyres, S. W., and M. H. Carr, Geomorphic evidence for the distribution of ground ice on
1546 Mars, Science, 231, 249– 252, 1986.

1547 Tanaka, K.L., 1986. The stratigraphy of Mars. J. Geophys. Res. 91, E139–E158.

1548 Toon, O. B., Segura, T., Zahnle, K., 2010. The formation of Martian river valleys by impacts.
1549 Annu. Rev. Earth Planet. Sci. 38, 303–22.

1550 Turcotte, D. L., and Schubert, G., 1982. Geodynamics applications of continuum physics to
1551 geological problems, Wiley, 450p.

1552 Van Maren, D. S., 2007. Grain size and sediment concentration effects on channel patterns of
1553 silt-laden rivers, Sedimentary Geology, 202, (1-2), 297-316.

1554 Van Maren, D. S., J. C. Winterwerp, Z. Y. Wang, Q. Pu, 2009. Suspended sediment dynamics
1555 and morphodynamics in the Yellow River, China, Sedimentology, 56 (3) 785-806.

1556 Walder, J.S., 2000a. Pyroclast/snow interactions and thermally driven slurry formation. Part 1:
1557 Theory for monodisperse grain beds. Bull. Volcan. 62, 105-118, DOI:
1558 10.1007/s004459900069

1559 Walder, J.S., 2000b. Pyroclast/snow interactions and thermally driven slurry formation. Part 2:
1560 Experiments and theoretical extension to polydisperse tephra. Bull. Volcan. 62, 119-129, DOI:
1561 10.1007/s004459900070.

1562 Warner et al. 2010a, Late Noachian to Hesperian climate change on Mars: Evidence of
1563 episodic warming from transient crater lakes near Ares Vallis, *JGR-planets,* Doi:
1564 10.1029/2009JE003522.

1565 Warner et al. 2010b, Hesperian equatorial thermokarst lakes in Ares Vallis as evidence for transient
1566 warm conditions on Mars, *Geology*, v. 38

1567 Werner, S., 2008 The early martian evolution - Constraints from basin formation ages, Icarus,
1568 195 (1) 45-60 , DOI: 10.1016/j.icarus.2007.12.008.

1569 Werner, S.C., Tanaka, K.L., 2011. Redefinition of the crater-density and absolute-age
1570 boundaries for the chronostratigraphic system of Mars, Icarus, doi:
1571 10.1016/j.icarus.2011.07.024.

1572 Williams R.M.E., Malin, M.C., 2008, Sub-kilometer fans in Mojave Crater, *Icarus* 198, 365–
1573 383.

1574 Wood, L.J., 2006. Quantitative geomorphology of the Mars Eberswalde delta, GSA Bulletin,
1575 118 (5/6) 557–566.

1576 Wray, J. J., R. E. Milliken, C. M. Dundas, G. A. Swayze, J. C. Andrews-Hanna, A. M.
1577 Baldridge, M. Chojnacki, J. L. Bishop, B. L. Ehlmann, S. L. Murchie, R. N. Clark, F. P. Seelos,
1578 L. L. Tornabene, S. W. Squyres, 2011. Columbus crater and other possible groundwater-fed
1579 paleolakes of Terra Sirenum, Mars Journal of Geophysical Research-Planets, vol. 116,
1580 E01001, 41 PP., doi:10.1029/2010JE003694.

1581 Xu, J., 2002, Complex behaviour of natural sediment-carrying streamflows and the
1582 geomorphological implications, 27 (7) 749–758.

1583

1584

1585

1586

1587

1588

Tab. 1: Crater frequencies and their model absolute ages for lower boundaries of Martian epochs at specific crater diameters in cumulative numbers. For the fits different size-frequency distribution shapes were used: (a) a minus-two-slope power law as in Werner and Tanaka (2011), (b) the description by *Ivanov (2001),* and (c) a cumulative version of the description by *Hartmann (2005)*. The age is derived from the chronology model of (b) *Ivanov (2001),* and (c) derived from *Hartmann (2005)*. The anchor points are printed in bold. Epochs boundary defined from N(5) and N(16) not shown here. See Werner and Tanaka (2011) for details.

	Model ages (Ga)		N(1)			N(2)		
Epoch boundaries	b	c	a	b	c	a	b	c
Mid-Late Amazonian	0.39	0.23	**160**	**160**	**160**	40	24	33
Early-Mid Amazonian	1.45	0.88	**600**	**600**	**600**	150	88	122
Hesperian–Amazonian	3.46	3.00	**2100**	**2100**	**2100**	525	309	427
Early-Late Hesperian	3.65	3.40	3125	4050	3067	781	597	624
Noachian–Hesperian	3.74	3.57	5000	6481	4097	1250	955	998
Mid-Late Noachian	3.86	3.85	25600	12667	19315	6400	1866	3930
Early-Mid Noachian	3.97	3.96	51200	25334	38630	12800	3733	7859

Fig. 1: Holden and Eberswalde location on global MOLA map (a). (b) Broad context from a combination of THEMIS daytime mosaic and HRSC nadir images with MOLA altimetry in color. (c) Detail of HRSC mosaic over Holden and Eberswalde craters.

Fig. 2: Holden and Eberswalde morphological mapping. (a) THEMIS daytime mosaic for context. (b) Map of Holden ejecta and fluvial valleys. Ejecta boundaries are defined using observations of megabreccia and rays/grooves on the continuous ejecta blanket centered on Holden. North is up.

Fig. 3: (a) HRSC mosaic of Holden northern ejecta (see box in figure 1). Dashed lines labeled “CEB” correspond to continuous ejecta boundary. (b) to (f) Close-up on Holden ejecta with megabreccia in MOC images S14-02902 (b), R12-03627 (c and d), R16-01387 (e), HiRISE images PSP 03222_1565 (f) and PSP 002233_1560 (g). (g) is located inside Eberswalde depression with a sinuous inverted channel covering breccia blocks unit. S: secondaries. B: breccia blocks. North is up.

Fig. 4: Crosscutting relationships between Eberswalde feeding valleys and ejecta. (a) HRSC image orbit 4199 of part of the Eberswalde fan watershed. Dotted lines indicate approximate boundary of Eberswalde ancient crater rim. (b) HiRISE image ESP13599_ 1560 close-up one of the main channel showing erosion cut through brecciated unit. (c) MOC image R1500025 close-up of channel and a crater showing brecciated unit in the bedrock (d) MOC image R1601387 of the main tributary before reaching Eberswalde fan showing erosion through brecciated unit. Valley depth here reaches 150 m showing ejecta thickness may reach 150 m in. B: Largest breccia blocks. North is up.

Fig. 5: Crosscutting relationships between Holden secondary craters and ancient valley networks. HRSC close-up (orbit numbers 2493 and 0511) of three areas where chains of secondaries have impacted former valley networks (a and b) and a large valley connecting to Ladon basin (c). North is up. See boxes in figure 1 for context.

Fig. 6: Crater counts of northern Holden ejecta blanket and interior using HRSC and CTX images. Left: Incremental plot on Hartmann isochrons. The red point corresponds to the 16 km diameter crater (Crater Bigbee) on the rim of Holden. Right: Same count plotted in Neukum's system with interpolated model age obtained using craters >700 m for Holden ejecta and >1.4 km for Holden interior.

Fig. 7: (a) HRSC images on Eberswalde and NW Holden ejecta (#7233 on the left, #4310 on the right). Same extent as figure 3a. (b) Map of valley networks on NW Holden ejecta from manual mapping. (c) HRSC DEM on Eberswalde and NW Holden ejecta with a spatial grid of 60 $m.pixel^{-1}$ (d) Map of valley networks on NW Holden ejecta performed by semi-automatic DNR HYDRO software using HRSC DEM (e) MOLA altimetry on Eberswalde and NW Holden ejecta. Contour interval 100 m. (f) Map of valley networks on NW Holden ejecta performed by semi-automatic DNR HYDRO software using MOLA DEM. 1. Contour lines spaced of 100 m, 2. Boundary of impact craters, 3. Valleys, 4. Watershed divide, 5. Eberswalde delta, 6. Eberswalde paleolake with a level at -1300 m in elevation taken as an uppermost lake elevation from the fan deposits elevation. CEB: Continuous ejecta boundary.

Fig. 8: Close-ups on Eberswalde fan deposits. (a) CTX image P01_001336_1560 showing an overall view of the fan (b) to (e) Close-ups from HiRISE image PSP_1534_1560. Individual channel deposits can be seen with block deposits (BD) corresponding to channel fill strata intercalated with finer grained sediments. Note 20 m wide polygons cross fine-grained sediments but not coarser deposits..

Fig. 9: Fan delta model scenarios for the Eberswalde setting, showing cross-sectional profiles of the entire crater with the true and modeled deposit (top graphs, magnified in middle graphs) and the time-evolution of the modeled fan (bottom graphs). Modeled crater (drawn in red) approximates the hypsometry of the real crater (in green). Measured profiles are shown along the central axis of the deposit (green) and 30^{o} left and right of the axis from the fan apex (blue and red). The modeled delta deposits are drawn (straight black lines) for some time steps at the prescribed angles of the fluvial topset and deltaic foreset, and blue dots at their intersections are shoreline positions. Time series (bottom graphs) show shoreline position (delta width) normalized by crater diameter *D* and water level above the crater floor normalized by the crater depth *d*. For the dilute flow scenario (left) the lake water level is determined by an imposed overflow level and most of the water influx escapes from the lake. For the dense flow scenario (right) the lake water level is determined by the water and sediment influx and the event duration. See Appendices for details.

Fig. 10: Top: Cooling of a 100 m thick ejecta (dotted line) with initial temperature of 300 °C. Results show that a ~60 m thick substratum can be heated above water melting point in ~150 years. Middle: Cooling of a 100 m thick ejecta (dotted line) with initial temperature of 600 °C. Results show that a ~120 m thick substratum can be heated above water melting point in ~300 years. Bottom: Cooling of a 200 m thick

ejecta (dotted line) with initial temperature of 600 °C. Results show that a ~240 m thick substratum can be heated above water melting point in ~1000 years. See Mangold (2012) for explanations.

Fig. 11. Output from a 1D column Stefan model of ejecta melting of water ice in Eberswalde's catchment. Solid black line corresponds to the cumulative discharge across the main Eberswalde fan, from a model run with ejecta average temperature *T* = 200°C. The dotted line corresponds to the water volume in the lake with a combined loss rate (sublimation + infiltration) of 0.1 m/yr from a 600 km2 lake surface (8 W/m^2 if all sublimation). The dashed line corresponds to the water volume in the lake with a combined loss rate of 1 m/yr (80 W/m^2 if all sublimation). The thick gray horizontal lines correspond to the volume needed to fill Eberswalde to two threshold elevations: -1400m (approximately the base of the main Eberswalde fan), and -1350m (most of the way up the main Eberswalde fan).

Fig. 12: Summary of the chronology obtained in this study, including ages proposed by Schultz (1982), Grant and Parker (2002), Werner (2009) and Grant and Wilson (2011) for landforms not focused in the present study (Uzboï, Ladon, Holden basin). Absolute ages according Ivanov (2001) model in bold and Hartmann (2005) in italic. EN/ Early Noachian. MN: Middle Noachian. LN: late Noachian. EH: Early Hesperian. LH: Late Hesperian: EA: Early Amazonian.

1706 Highlights:

1707 Valleys feeding the Eberswalde fan crosscut Holden impact crater ejecta blanket.

1708 Holden crater formation likely postdates the Early Hesperian.

1709 Modeling shows Eberswalde fan can form at a geologically rapid rate.

1710 The role of Holden crater in Eberswalde fluvial activity is highlighted.

1711

1712

Figure 1

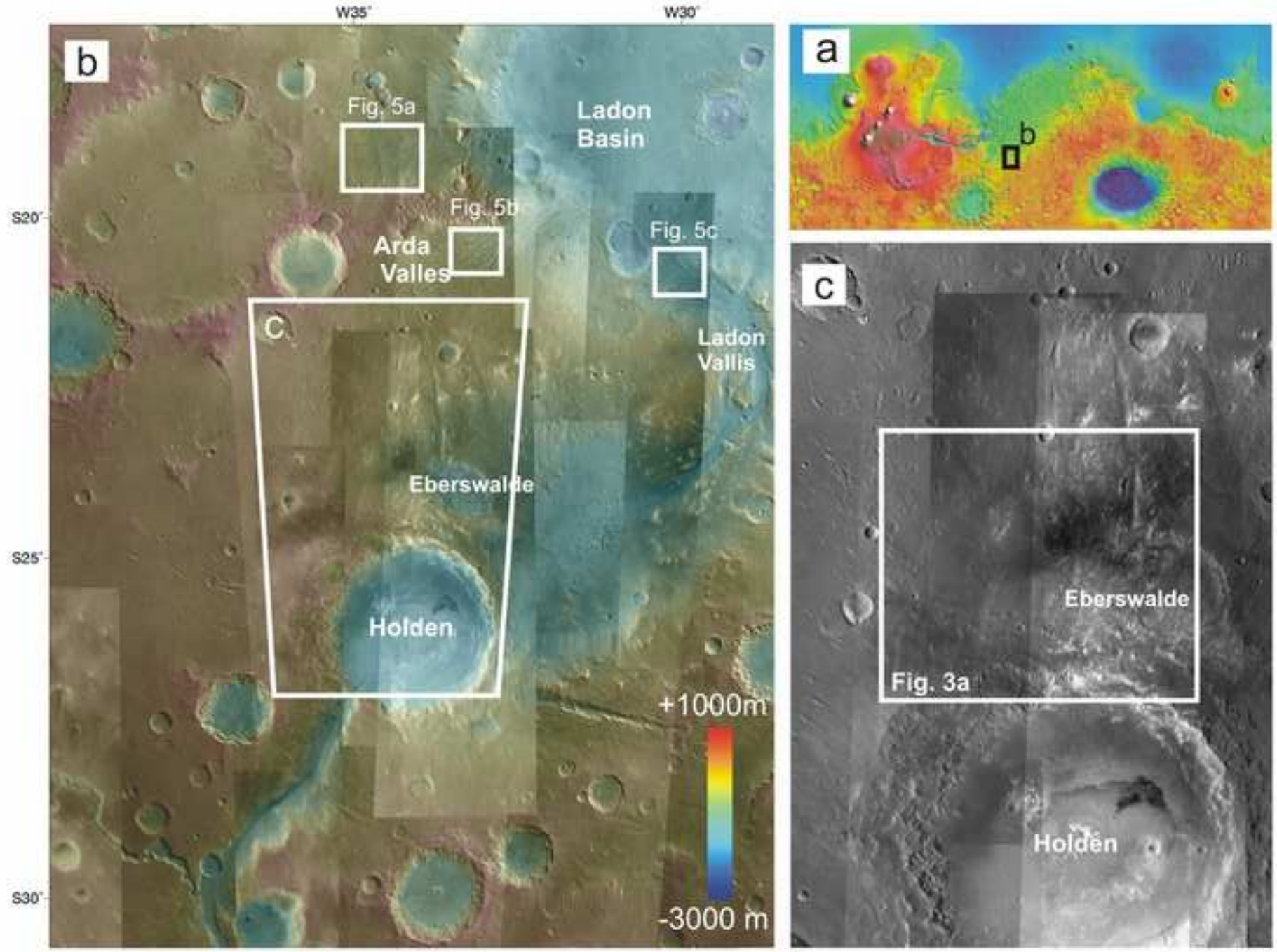

Figure 2

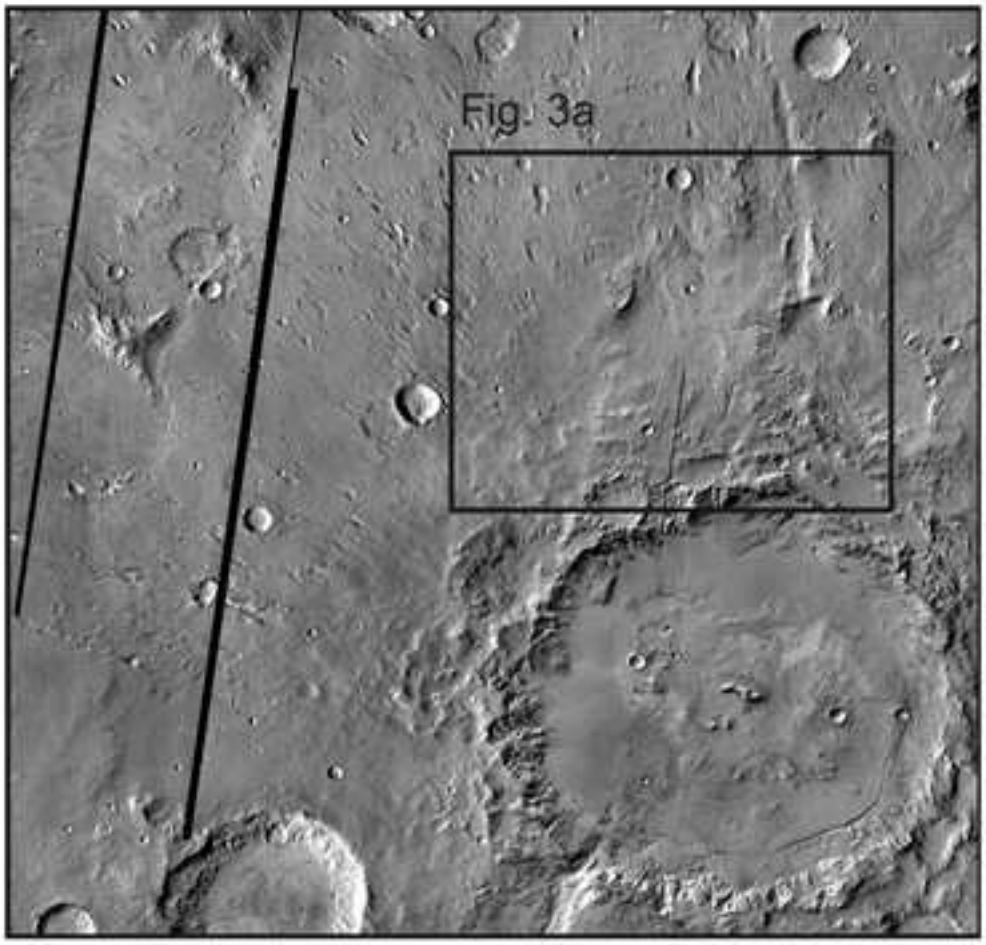

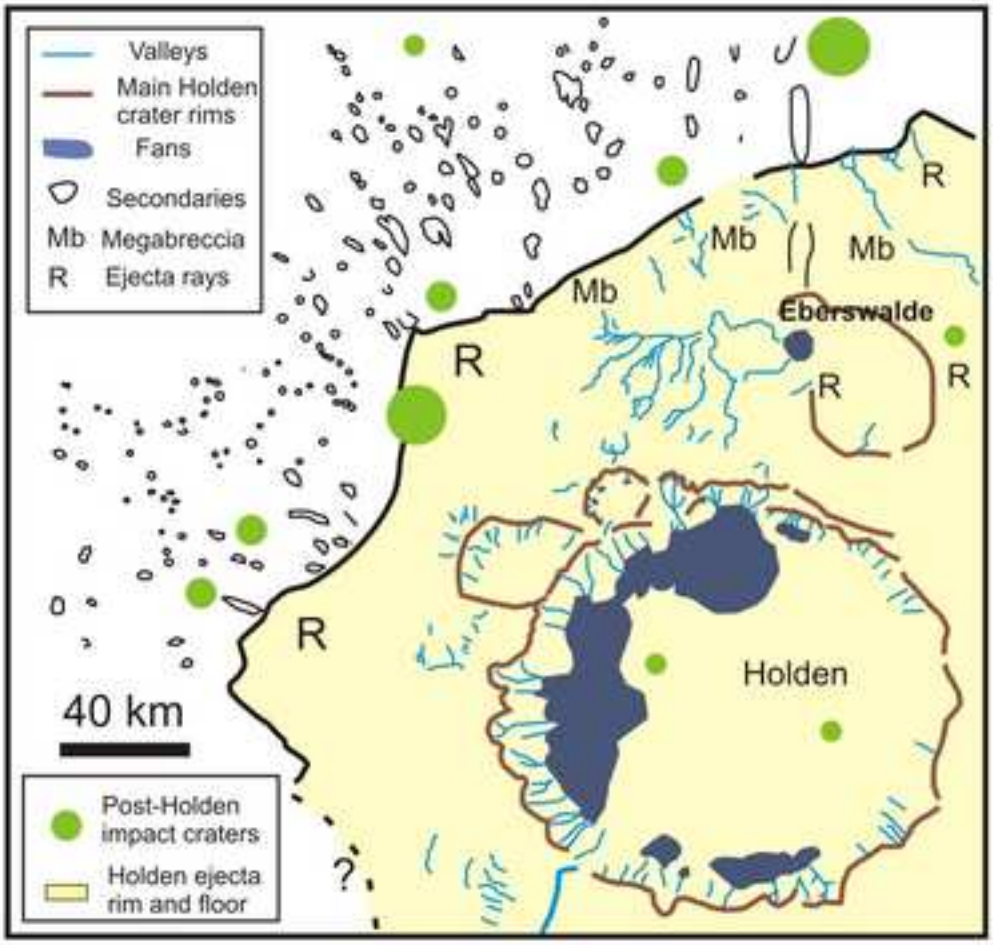

Figure 3

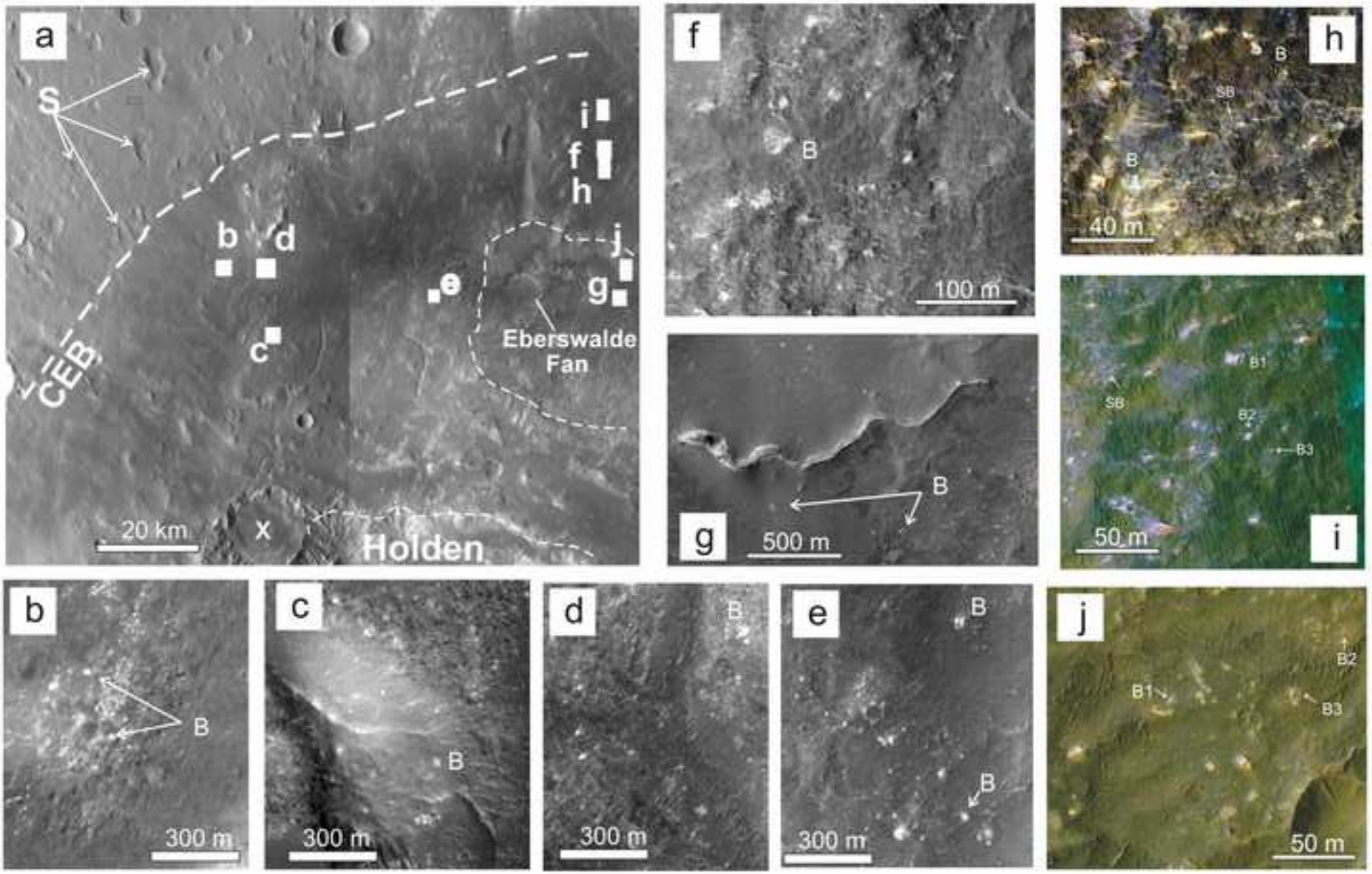

Figure 4

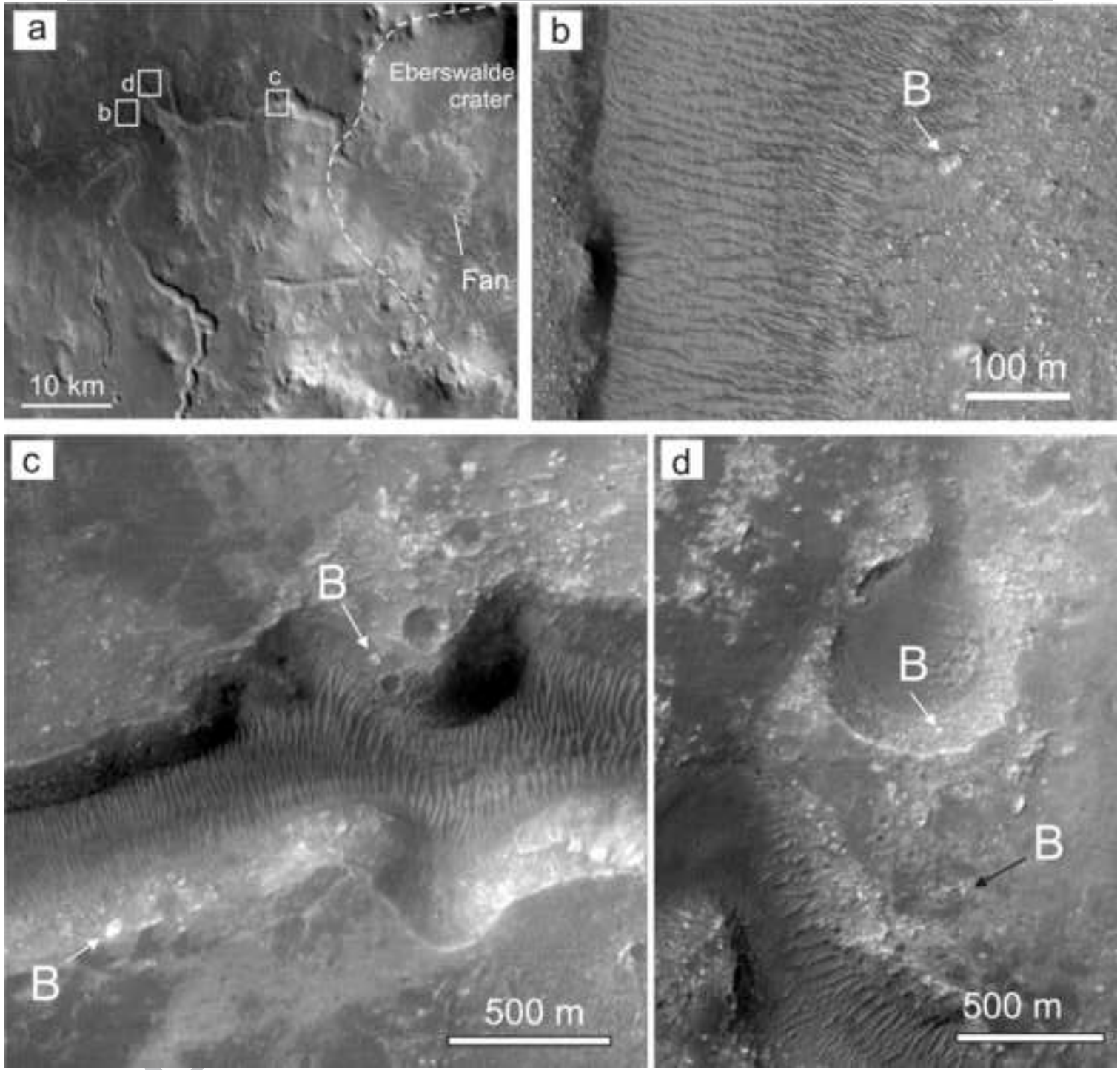

Figure 5

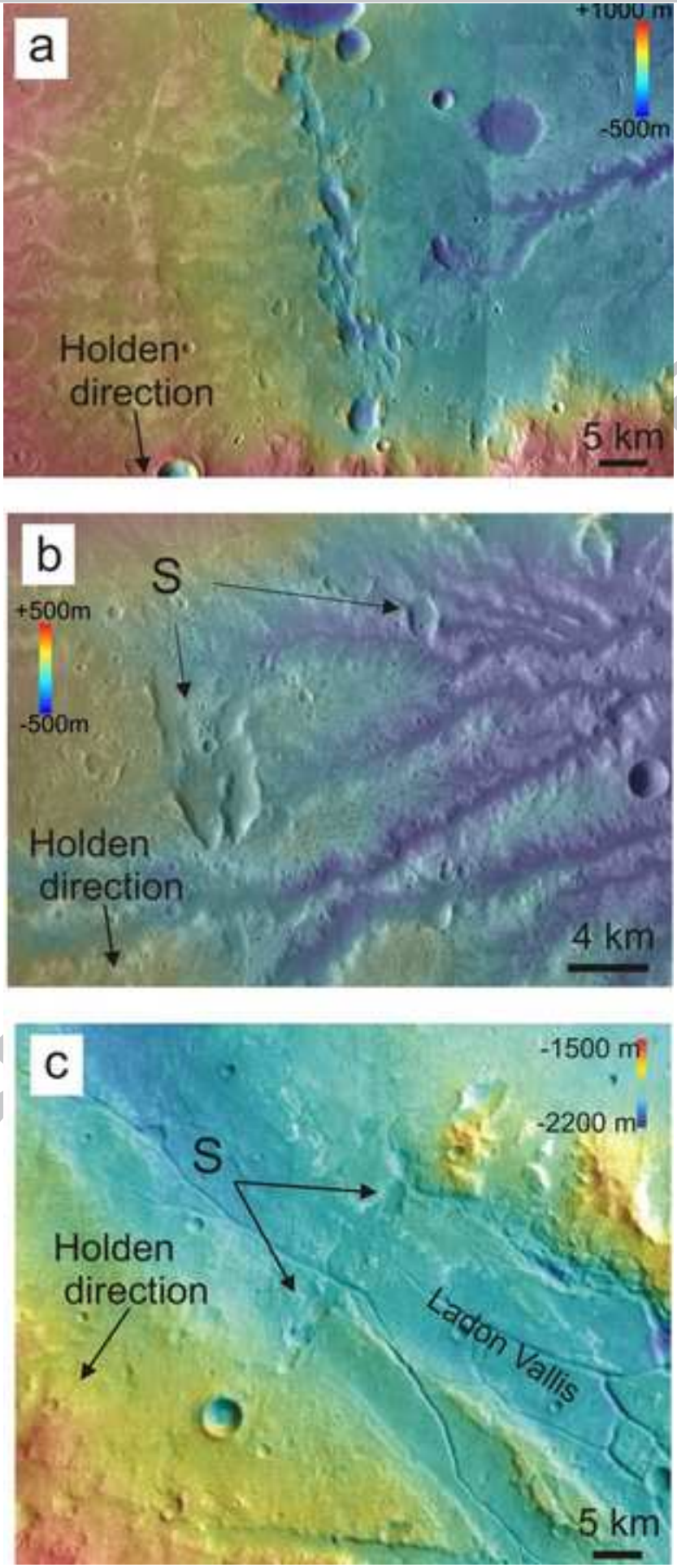

Figure 6

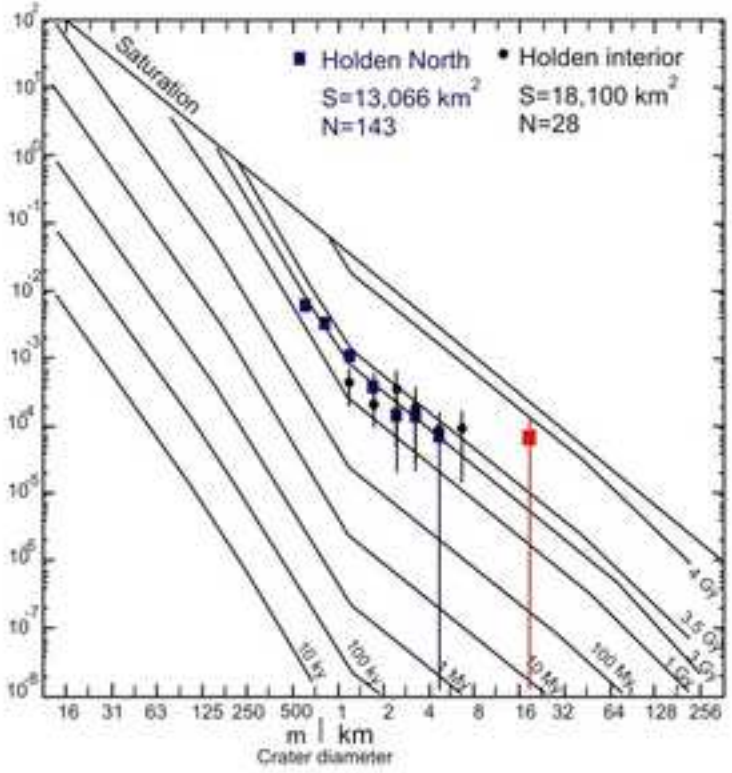

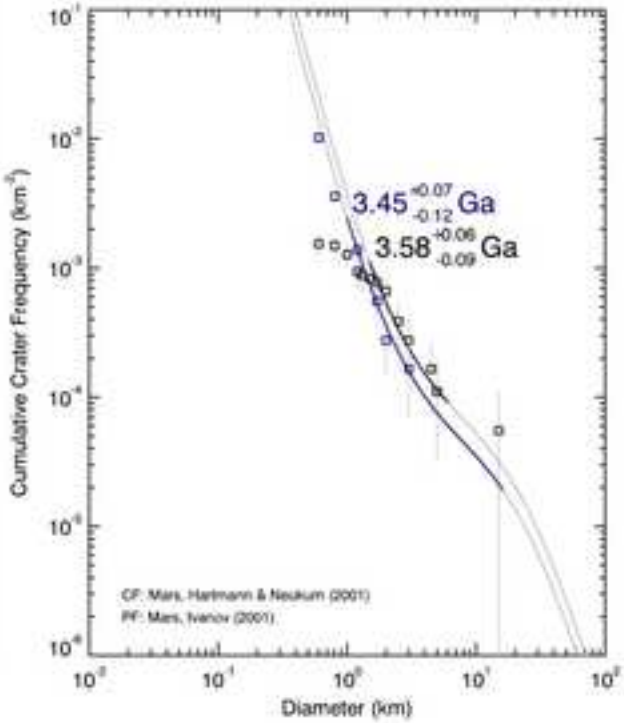

Figure 7

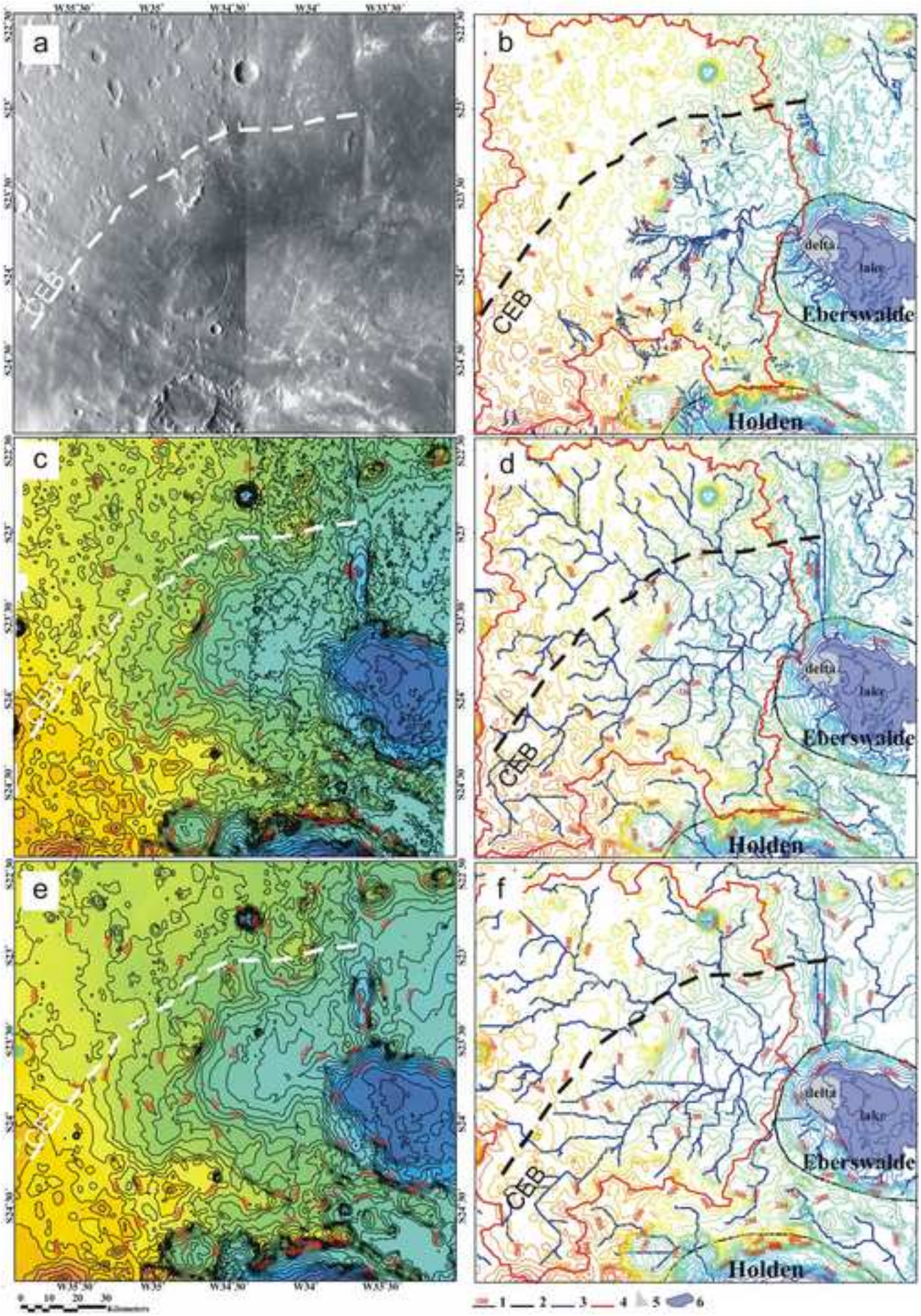

Figure 8

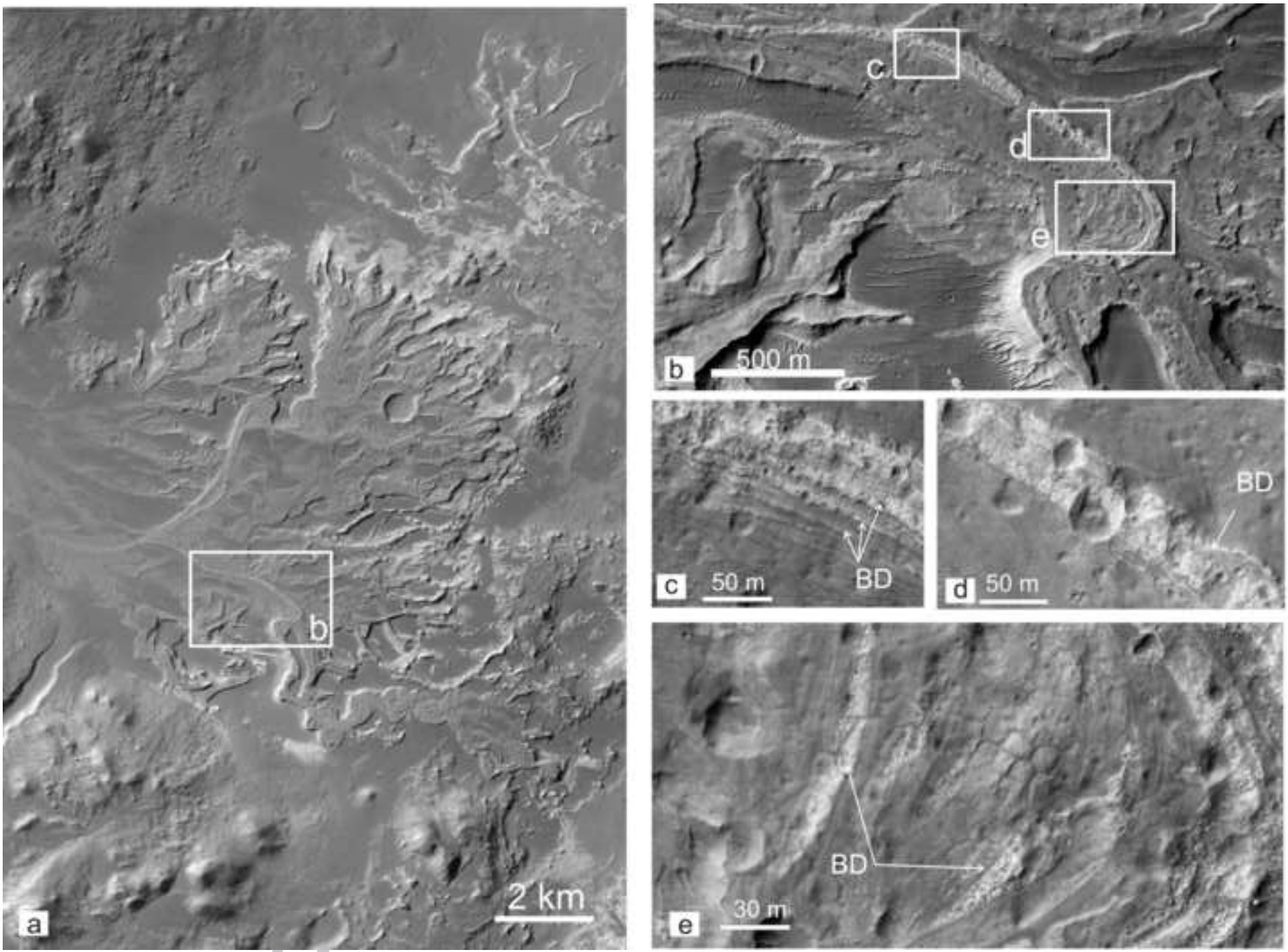

Figure 9

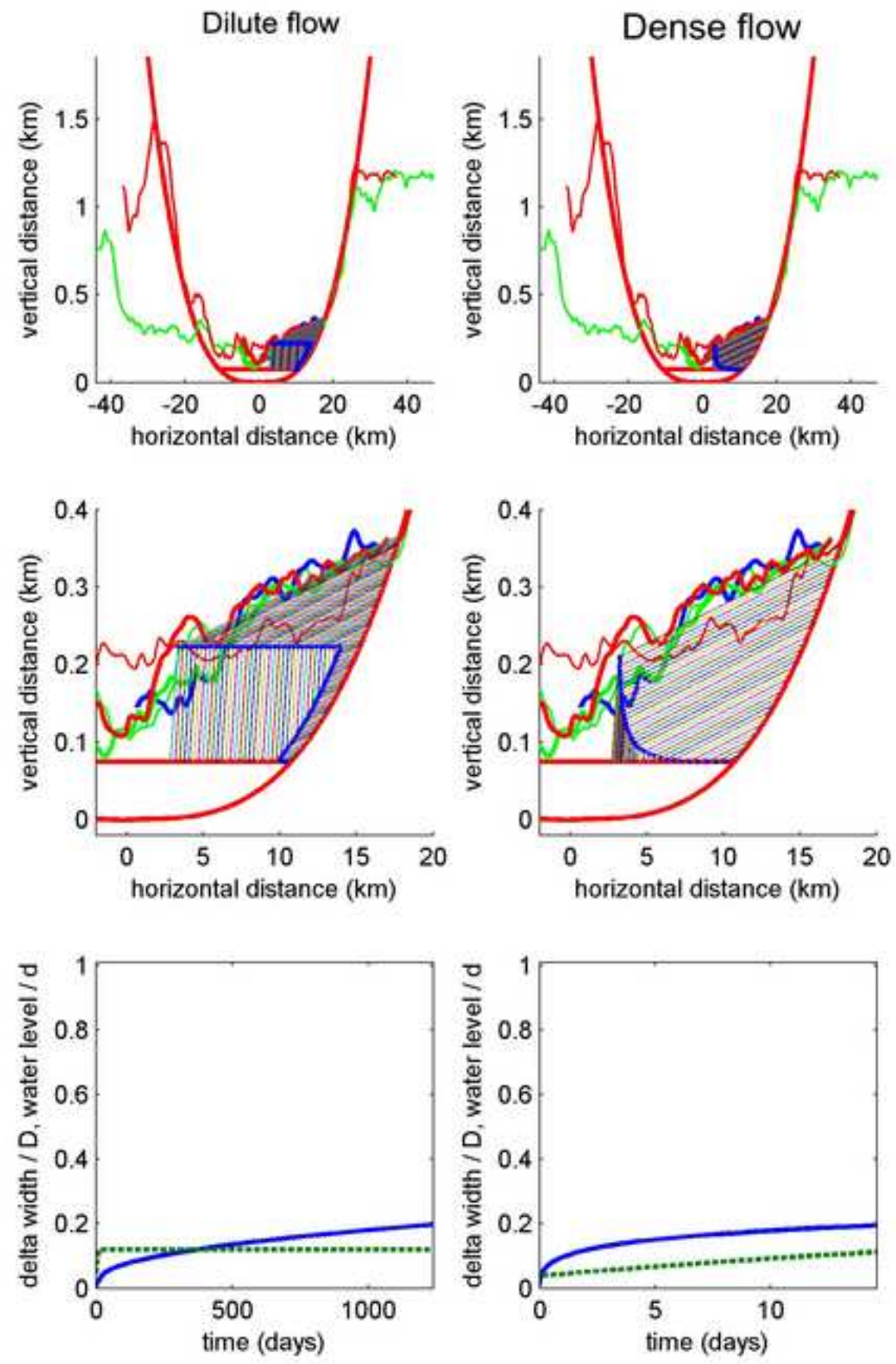

Figure 10

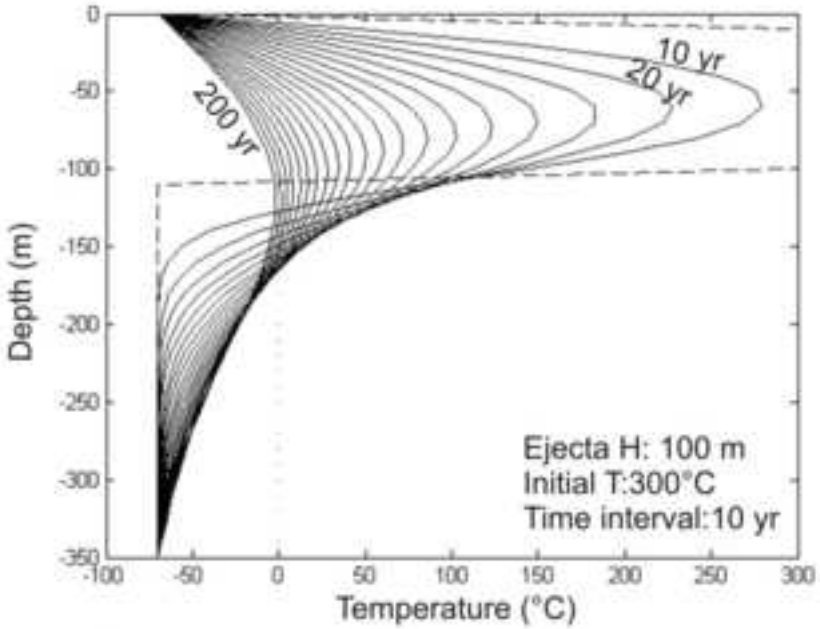

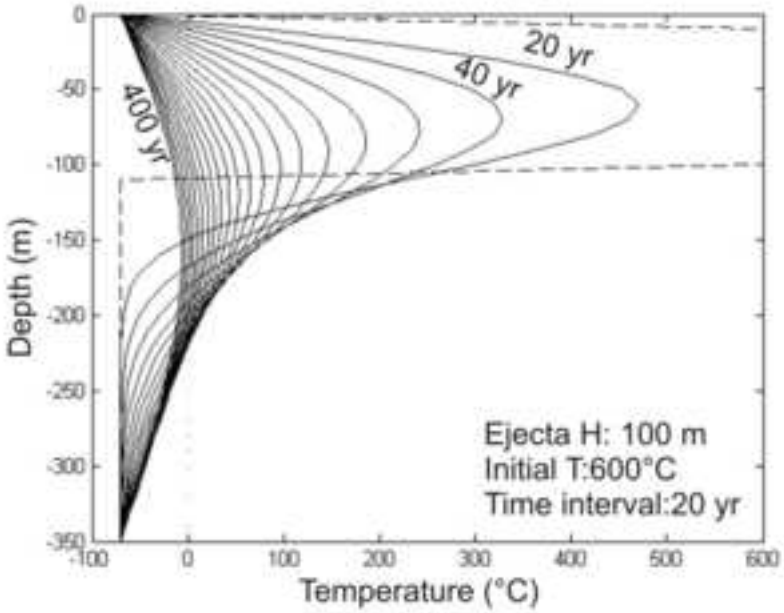

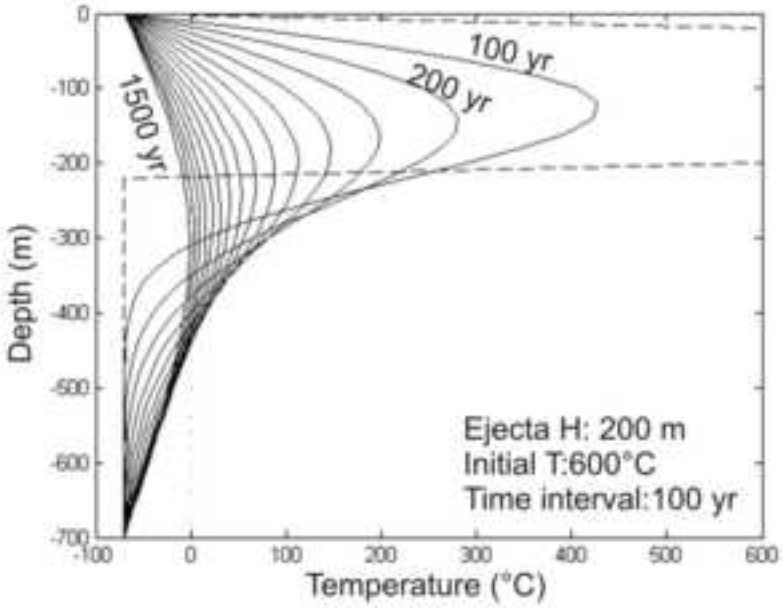

Figure11

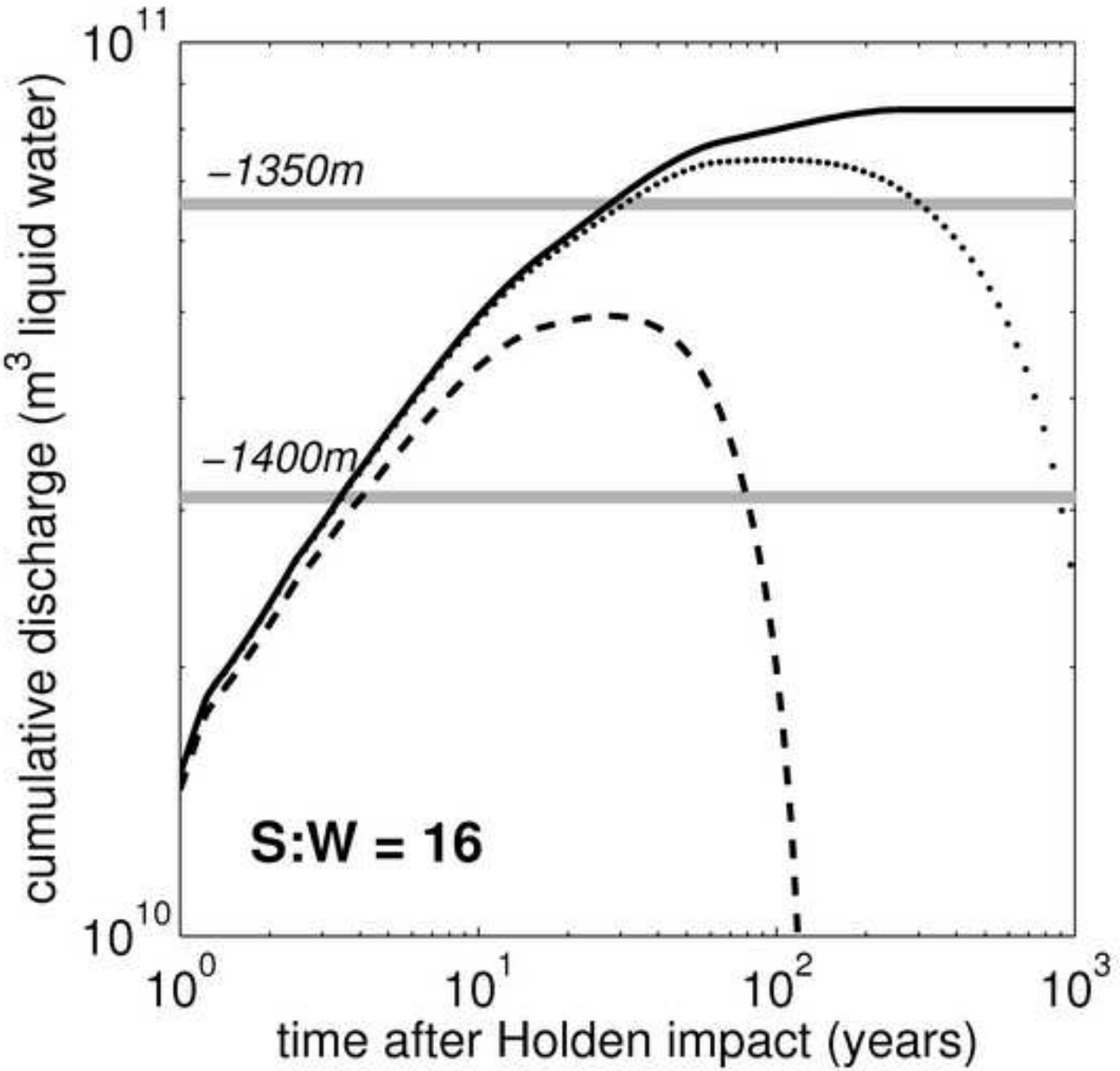

Figure 12